1971

Spectroscopic temperature measurements of flames and their physical significance

Isaac Reif
Iowa State University

Spectroscopic temperature measurements of flames and their physical significance

by

Isaac Reif

A Dissertation Submitted to the
Graduate Faculty in Partial Fulfillment of
The Requirements for the Degree of
DOCTOR OF PHILOSOPHY

Major Subject: Physical Chemistry

Approved:

Signature was redacted for privacy.

In Charge of Major Work

Signature was redacted for privacy.

Head of Major Department

Signature was redacted for privacy.

Dean of Graduate College

Iowa State University
Ames, Iowa

1971

TABLE OF CONTENTS

I. INTRODUCTION

When aerosols of metal salt solutions are introduced into appropriate flames, free atoms of most metallic elements are formed in sufficient abundance to allow their detection and quantitative determination, at solution concentrations of the order of parts per million, by atomic absorption, emission, or fluorescence techniques. As a consequence, simple combustion flames are now one of the most useful devices available to the analytical chemist for the determination of trace elements in solution. Flames also enjoy a wide popularity as spectroscopic sources for the study of collisional and radiative processes.

An accurate knowledge of flame temperatures is a prerequisite to the definitive understanding of flame reaction rates and propagation mechanisms, the disposition of various dissociation and ionization equilibria involving the natural flame species, and the processes involved in the atomization, excitation and ionization of flame additives. The need for high accuracy in flame temperature measurements is related to the fact that relevant quantities, such as kinetic rate constants or populations of excited states, follow an exponential temperature dependence of the type

$$P = C\, e^{-E/kT}$$

where P is some chemical or physical parameter, C is a constant, E is an energy and k is Boltzmann's constant. Some

relative errors introduced into P by small errors in the measured temperature dT calculated from the expression

$$\frac{dP}{P} = \frac{E}{kT^2}\, dT$$

are summarized in Table 1 for a source at 3000°K. It is seen, for example, that only a 50°K error in the temperature (which amounts to only an ~1.5% error in the measurement) could give rise to a 30% or greater error in P, depending on the energy term. At 2000°K, the error values would increase by more than a factor of two.

Table 1. Relative errors introduced by small errors in measured temperatures

$(\frac{dP}{P} \times 100)$ at T = 3000°K

Energy (cm^{-1})	ΔT(K) 10	20	30	40	50
1000	0.2	0.3	0.5	0.6	0.8
5000	0.8	1.6	2.4	3.2	4.0
10000	1.6	3.2	4.8	6.4	8.0
20000	3.2	6.4	9.6	12.8	16.0
30000	4.8	9.6	14.4	19.2	24.0
40000	6.4	12.8	19.2	25.6	32.0

In spite of this need for accuracy, it is not uncommon for investigators to employ temperature measurements with apparent errors of ± 50°K, ± 100°K, or even ± 200°K (1,2,3) as a basis for flame calculations and interpretations. The uncertainties inherent in many of the published flame temperature

data can be traced to fundamental limitations in the method of measurement and/or to unjustified liberties taken in their execution.

Spectroscopic techniques are commonly used for the measurement of flame temperatures primarily because these methods do not disturb the combustion process. Moreover, these techniques may be the only applicable methods if the temperatures are high or if the flame system is inaccessible to probes. Among the various spectroscopic techniques, the line reversal (4-9), emission-absorption (10-14), slope (11,15-17), and two-line methods (2,18) are used most extensively. Temperature measurements performed by any of these techniques are subject to experimental and systematic errors, even if isothermal flames with uniform concentrations of the spectroscopic thermometric species are considered. For actual flames, i.e., those possessing temperature and concentration gradients of the thermometric species, the temperature value measured, though it may be very precise, may not have real physical significance. The importance of the bias that these non-homogeneities may exert on the measured spectroscopic temperatures has received increasing attention, especially during the past 10 years, and several important papers have been published (19-29) on the subject. However, several very important questions have not been answered definitively and many promising lines of inquiry are open for additional

investigations. The nature of these questions and lines of inquiry will become apparent as we review the theoretical basis for the various techniques and identify existing gaps in our knowledge.

II. TEMPERATURE, THERMODYNAMIC EQUILIBRIUM, AND LOCAL THERMAL EQUILIBRIUM

In a strict sense, a temperature T may only be defined for systems in thermodynamic equilibrium. For the latter to exist, a unique value of T must be sufficient to describe (30):

a) The velocity distribution function of all the particles according to Maxwell's equation.

b) The population of the excited states according to Boltzmann's equation.

c) The distribution of molecules and their dissociation products according to the mass action law of Guldberg and Waage.

d) The distribution of atoms and their ionization products according to the Saha-Eggert's equation.

e) The distribution of the electromagnetic radiation field according to Planck's law.

However, general thermodynamic equilibrium does not prevail in flames (31,32,33). In the primary reaction zone of the flame, the gas molecules do not spend enough time to allow the equipartition of the chemical energy released by the oxidation reactions among the various degrees of freedom. As the molecules enter the secondary reaction zone, the equilibration of the translational and rotational degrees of freedom is established almost immediately, but the vibrational and electronic degrees of freedom proceed more slowly and the ioniza-

tion and chemical equilibria may not be accomplished (31).

Although the major stable flame species leave the primary reaction zone with concentrations not very different from their equilibrium values, the radicals usually enter the secondary reaction zone at supra-equilibrium concentrations. As a result of radical recombination reactions, more chemical energy is released and a temperature gradient is established in the vertical axis. Turbulent or diffusive mixing of the flame gases with the surrounding atmosphere also contributes to a non-uniform distribution of temperature in the horizontal plane.

The flame radiation cannot be described by Planck's function because it is often transparent over large wavelength regions. Only the radiation field in a blackbody source follows Planck's distribution. Thus, radiation equilibrium may exist only in the central part of the flame and at the wavelength center of strong resonance lines. This lack of radiative equilibrium produces a depopulation of the upper energy levels with respect to the lower ones, because atoms and molecules are deexcited by emission of radiation and inelastic collisions but the excitation, since selfabsorption is relatively small, occurs almost only by inelastic collisions. Nevertheless, the extent of this depopulation effect is very small for most flames at atmospheric pressure because collisional induced transitions are much more frequent than

radiative ones (4).

Despite all of these deviations from thermodynamic equilibrium, the very useful concept of local thermal equilibrium can be employed in flames (31). A system is in thermal equilibrium when the distribution of the velocity of the particles and the population of their energy levels can be described by a single value of a temperature T. This concept can be extended to include situations where thermal equilibrium is established at each point in the flame but allowing the possibility of different temperatures at different points. Thus, we may speak of a state of local thermal equilibrium characterized by local temperatures. The state of local thermal equilibrium is reached when the rate at which the energy is equipartitioned over the different degrees of freedom is much faster than the rate of transport of heat, radiation and mass through the flame.

In the discussion that follows we will limit ourselves to temperature measurements in flames characterized by a state of local thermal equilibrium.

III. THEORETICAL CONCEPTS

A most desirable starting poi for a systematic evaluation of spectroscopic temperature measurements of flames is a unifying discussion and development of theoretical concepts. In the theoretical discussion that follows, the basic theoretical principles of temperature measurements of completely uniform flames (with no temperature or concentration gradients of the thermometric species) by each of the four commonly used spectroscopic techniques will be presented. Although most of the thought processes and theoretical concepts applicable to this idealized situation have been recorded in the literature, the following presentation of the theory allowed us to unify the nomenclature and notation, and to show the validity of each technique under idealized conditions. There have been only fragmentary and scattered accounts on the extension of the basic theory to the increasingly more complicated but realistic situations, i.e., isothermal, non-homogeneous and non-isothermal, non-homogeneous flames. The systematic development of the theory for these flames which follows the introductory treatment on uniform flames for each measurement technique constitutes a major contribution of this thesis.

Flame emission and flame absorption play an important role in the four methods for temperature measurements under study. The quantity related to emission or absorption that is measured in the laboratory is radiance, the power per unit

solid angle per unit area. The general expressions for the emitted and absorbed radiances of a spectral source characterized by local thermal equilibrium are given by the solutions of the differential equation of radiative transfer (34),

$$B(em) = \int_{\Delta\nu_{qp}} d\nu \int_0^{\ell} dx \left(\frac{1}{4\pi} A_{qp} h\nu n_q P(\nu)\right) e^{-\int_0^x dx' K(\nu)} \quad (1)$$

$$B(abs) = \int_{\Delta\nu_{qp}} d\nu B_\nu^b(\nu, T_b) \left(1 - e^{-\int_0^{\ell} dx K(\nu)}\right) \quad (2)$$

where $K(\nu) = \frac{h\nu}{c} (B_{pq} n_p - B_{qp} n_q) P(\nu)$ (3)

and ℓ = length of the optical path.

A_{qp}, B_{qp} and B_{pq} = spontaneous emission, induced emission and induced absorption transition probability coefficients.

n_q, n_p = particle density in the upper and lower quantum states of the transition.

$P(\nu)$ = line shape function.

$B_\nu^b(\nu, T_b)$ = spectral radiance of a black body source at temperature T_b and frequency ν.

T_b = brightness temperature of the source.[1]

---

[1] The brightness temperature of a source is defined as the temperature at which a blackbody emits the same spectral radiance as the source, at a given wavelength (7).

h = Planck constant.

c = speed of light.

The flame edge closest to the spectrometer is considered as the origin of the coordinates. The expression

$$dx\left(\frac{1}{4\pi} A_{qp}\ h\nu\ n_q\ P(\nu)\right)$$

then describes the spectral radiance of a volume differential of length dx at a distance x from the origin. The factor

$$e^{-\int_o^x dx' K(\nu)}$$

represents the fraction of the energy lost to selfabsorption as the light travels towards the edge. $P(\nu)$ is a normalized function which describes the shape of the line profile. This function is the same for emission and absorption in sources in local thermal equilibrium (34). The B coefficients are defined in terms of intensity of isotropic radiation (35).

A. The Line Reversal Method

1. Uniform flame

The most commonly used technique for measuring flame temperatures is based on equating the brightness temperature of a continuum source and the excitation temperature of the thermometric species in the flame, which may be either a natural flame molecule or an element introduced into the flame. The principles of this technique have been described in a number of publications (4-9). The actual temperature measurement is based on the optical "reversal" of the emission of an

appropriately selected spectral line by the continuum radiation generated in a temperature calibrated source. At the "reversal point" the radiant energy emitted by the flame is equal to the energy absorbed from the continuum. The reversal determination is generally achieved by scanning the selected spectral line past the exit slit of the spectrometer and comparing the recorded intensity at the line center and at the edges for various lamp currents, i.e. brightness temperatures of the lamp. No net emission or absorption of radiation should be observed at the reversal point.

The flame temperature can be shown to be equal to the lamp brightness temperature at the reversal point in the following manner. At the reversal point,

$$B(em) = B(abs)$$

In a uniform flame, $K(\nu)$ is independent of x and the integral in the exponents of Equations 1 and 2 can be evaluated directly. Thus,

$$B(em) = \int_{\Delta\nu_{qp}} d\nu \int_{c}^{\ell} dx \left(\frac{1}{4\pi} A_{qp}\, h\nu\, n_q\, P(\nu)\right) e^{-K(\nu)x} \qquad (4)$$

and

$$B(abs) = \int_{\Delta\nu_{qp}} d\nu\, B_{\nu}^{b}(\nu, T_r)\,(1-e^{-K(\nu)\ell}) \qquad (5)$$

where T_r stands for the brightness temperature of the continuum source at the reversal point. If Equation 4 is integrated with respect to x and the expression $K(\nu)$ in Equation 3 is substi-

tuted, the value of B(em) becomes

$$B(em) = \int_{\Delta\nu_{qp}} d\nu \frac{1/4\pi\ A_{qp}\ h\nu\ n_q\ P(\nu)}{\frac{h\nu}{c}(B_{pq}n_p - B_{qp}n_q)P(\nu)} (1-e^{-K(\nu)\ell})$$

This equation can be simplified by the use of the relationships between the transition probability coefficients (7),

$$\frac{A_{qp}}{B_{qp}} = \frac{8\pi h\nu^3}{c^3} \qquad \frac{B_{qp}}{B_{pq}} = \frac{g_p}{g_q}$$

and the Boltzmann population distribution,

$$\frac{n_q}{n_p} = \frac{g_q}{g_p} e^{-(E_q-E_p)/kT_f}$$

where E_q, g_q and E_p,g_p are the energies and degeneracies of the upper and lower quantum states, and T_f is the flame temperature. The resulting expression is

$$B(em) = \int_{\Delta\nu_{qp}} d\nu \left(\frac{c}{4\pi} \frac{8\pi h\nu^3}{c^3} \frac{1}{e^{h\nu/kT_f}-1} \right) (1-e^{-K(\nu)\ell})$$

where (E_q-E_p) has been substituted by $h\nu$. Since Planck's law is given by

$$B^b_\nu(\nu,T) = \frac{c}{4\pi} \frac{8\pi h\nu^3}{c^3} \frac{1}{e^{h\nu/kT}-1}$$

then

$$B(em) = \int_{\Delta\nu_{qp}} d\nu\ B^b_\nu(\nu,T_f)\ (1-e^{-K(\nu)\ell}) \qquad (6)$$

If B(em) is equal to B(abs) at the reversal point, then it is apparent from Equations 5 and 6 that T_r must equal T_f. Thus, the reversal method provides an accurate measurement of the flame temperature.

The reversal method has the advantage of being a null method, and therefore enjoys the high precision and accuracy common to all null measurements. Temperatures measured with an accuracy of $\pm$ 2°K at 2600°K by this technique have been reported in the literature (4). The method also has the advantages of not being affected by self-absorption, because the emission and absorption line profiles are affected in the same way for an isothermal flame. A third distinctive advantage of the line reversal method is that transition probability data are not required; these data are not known with the desired accuracy. The main disadvantage of the line reversal method is the need for a reference light source, generally a tungsten lamp, which must be: a) accurately calibrated; and b) capable of radiating at a brightness temperature at least equal to the flame temperature, otherwise the reversal point would be unattainable. Thus, the highest flame temperature which can be measured by this technique is determined by the highest brightness temperature attainable in the reference light source. There is also a need to satisfy several optical requirements: a) the acceptance angle of the spectrometer must be completely filled by continuum radiation, b) no flame

radiation should be reflected back into th optical path by the tungsten lamp; and c) the error introduced by temperature gradients in the lamp filament should be minimized by performing the measurement with the same emitting area observed for the lamp calibration. Any spectral line can be used for reversal measurements, but a relatively high optical depth[1] is required experimentally to obtain good precision and accuracy. Consequently ground state transitions are generally employed.

2. Isothermal flame with a non-homogeneous distribution of the thermometric species

When the distribution of thermometric species is non-homogeneous, the expressions relating to temperature measurements understandably become more complex. For the sake of simplicity, in non-uniform flames the assumption will be made that the angle of acceptance is so small that any temperature or concentration distribution of the flame gases can be regarded as a function only of the axial length x.

Equations 1 and 2, with the explicit recognition of the axial dependence of the concentration, become

$$B(em) = \int_{\Delta\nu_{qp}} d\nu \int_{o}^{\ell} dx\left(\frac{1}{4\pi} A_{qp}\, h\nu\, n_q(x)\, P(\nu)\right) e^{-\int_{o}^{x} dx' K(\nu,x')} \qquad (7)$$

[1]The optical depth is defined as the product $n_p f \ell$ where f is the oscillator strength for the line (36).

and

$$B(abs) = \int_{\Delta\nu_{qp}} d\nu \; B_\nu^b(\nu,T_r) \; (1-e^{-\int_o^\ell dx \; K(\nu,x)}) \tag{8}$$

The average value of n_o, the number density of particles in the ground state, may be defined as

$$\overline{n_o} = \frac{\int_o^\ell dx \; n_o(x)}{\int_o^\ell dx} = \frac{\int_o^\ell dx \; n_o(x)}{\ell} \tag{9}$$

Following the same procedure as for a uniform flame and with the use of Equation 9, the following expressions are obtained:

$$B(em) = \int_{\Delta\nu_{qp}} d\nu \; B_\nu^b(\nu,T_f) \; (1-e^{-\overline{K(\nu)}\,\ell}) \tag{10}$$

$$B(abs) = \int_{\Delta\nu_{qp}} d\nu \; B_\nu^b(\nu,T_r) \; (1-e^{-\overline{K(\nu)}\,\ell}) \tag{11}$$

where $\overline{K(\nu)} = \frac{h\nu}{c}(B_{pq} \; \overline{n_o} \; e^{-E_p/kT_f} - B_{qp} \; \overline{n_o} \; e^{-E_q/kT_f}) \; P(\nu)$

At the reversal point B(em) = B(abs) and consequently T_f must be equal to T_r. Thus, as long as the flame is isothermal, a non-homogeneous distribution of the thermometric species will not bias the flame temperature measurements. There are, however, very few isothermal flames. When the thermometric species are introduced into or occur only in the central parts of shielded flames, an isothermal environment may result if

the shielding indeed protects this flame from the temperature gradients at the edges. In most real flames, there is not only a non-isothermal distribution of temperature but a non-homogeneous distribution of thermometric species as well.

3. Non-isothermal flame with a non-homogeneous distribution of the thermometric species

When the flame temperature is not constant along the optical path the equations involved when self-absorption effects are not negligible become even more complex. This complexity arises because self-absorption in a non-isothermal source does not affect the emission and absorption line profiles in the same way (19). The extent of the difference depends on the specific line shape, which is determined by the convoluted effect of Doppler, collisional and natural broadening processes. Thus, calculations may be applied only to specific lines, as has been done by Sasaki for the sodium D line (19). The utility of applying a simplifying assumption to this problem has not been generally recognized. If the tacit assumption is made that self-absorption effects are negligible, a very useful expression may be derived in the following way:

At very small values of $K(\nu,x)$,

$$e^{-\int_0^x dx' \, K(\nu,x')} \simeq 1$$

and

$$(1-e^{-\int_o^{\ell} dx\ K(\nu,x)}) \simeq \int_o^{\ell} dx\ K(\nu,x)$$

Consequently, Equations 7 and 8 can be written as

$$B(em) = \int_{\Delta\nu_{qp}} d\nu \int_o^{\ell} dx \left(\frac{1}{4\pi} A_{qp}\ h\nu\ n_q(x)\ P(\nu)\right)$$

and

$$B(abs) = \int_{\Delta\nu_{qp}} d\nu\ B^b\ (\nu,T_r) \int_o^{\ell} dx\ K(\nu,x)$$

Substituting the expressions for $K(\nu,x)$ and $B^b(\nu,T_r)$, and making use of the Boltzmann distribution equation,

$$B(em) = \int_{\Delta\nu_{qp}} d\nu \int_o^{\ell} dx\ \frac{1}{4\pi} A_{qp}\ h\nu\ n_o(x)\ \frac{g_q}{g_o}\ e^{-E_q/kT(x)} P(\nu)$$

$$B(abs) = \int_{\Delta\nu_{qp}} d\nu \left(\frac{c}{4\pi}\ \frac{8\pi h\nu^3}{c^3}\ \frac{1}{e^{\frac{h\nu}{kT_r}}-1}\right) \int_o^{\ell} dx\ \frac{h\nu}{c}$$

$$\left(B_{pq}\ n_o(x)\ \frac{g_p}{g_o}\ e^{-E_p/kT(x)} - B_{qp}\ n_o(x)\ \frac{g_q}{g_o}\ e^{-E_q/kT(x)}\right) P(\nu)$$

If the integration over the frequency is performed with $\nu \simeq \nu_o$ and the expressions for A_{qp} and B_{qp} are substituted, then

$$B(em) = \frac{1}{4\pi} \left(\frac{8\pi h\nu_o}{c^3}\ \frac{g_p}{g_q} B_{pq}\right) h\nu_o\ \frac{g_q}{g_o} \int_o^{\ell} dx\ n_o(x)\ e^{-E_q/kT(x)} \quad (12)$$

$$B(abs) = \frac{c}{4\pi} \frac{8\pi h\nu_o^3}{c^3} \left(\frac{1}{e^{E_q - E_p/kT_r} - 1}\right) \frac{h\nu_o}{c} \frac{g_p}{g_o} B_{pq}$$

$$\int_o^{\ell} dx\left(n_o(x) e^{-E_p/kT(x)} - n_o(x) e^{-E_q/kT(x)}\right) \tag{13}$$

At the reversal point these two expressions must be equal. Thus, simplifying

$$\left(\frac{1}{e^{E_q - E_p/kT_r} - 1}\right) \int_o^{\ell} dx\left(n_o(x)\, e^{-E_p/kT(x)} - n_o(x) e^{-E_q/kT(x)}\right) = \int_o^{\ell} dx\, n_o(x)\, e^{-E_q/kT(x)} \tag{14}$$

If the weighted average of the function $e^{-E/kT(x)}$ over the optical path is defined as

$$\overline{e^{-E/kT}} = \frac{\int_o^{\ell} dx\, n_o(x)\, e^{-E/kT(x)}}{\int_o^{\ell} dx\, n_o(x)} \tag{15}$$

it is possible to define a very useful parameter, $\dot{T}$, by the following relationship,

$$e^{-E/k\dot{T}} = \overline{e^{-E/kT}} \tag{16}$$

Thus, $\dot{T}$ represents the value of a parameter which substituted in the expression $e^{-E/k\dot{T}}$, gives the weighted average value of this function over the optical path. Obviously, the value of $\dot{T}$ depends on the particular temperature profile and concentration distribution of the thermometric species

under consideration. Just as significant, substitution of different values of the excitation energy into Equations 15 and 16 has shown that $\dot{T}$ is dependent on E as well. Thus, the notation $\dot{T}_{(E)}$ will be used to recognize explicitly this important energy dependence.

If Equations 15 and 16 are substituted into Equation 14, then

$$\left(\frac{1}{e^{E_q-E_p/kT_r}-1}\right)\left(e^{-E_p/k\dot{T}(E_p)}-e^{-E_q/k\dot{T}(E_q)}\right)=e^{-E_q/k\dot{T}(E_q)}$$

Rearranging,

$$\frac{1}{e^{E_q-E_p/kT_r}-1}=\frac{1}{e^{E_q/k\dot{T}(E_q)-E_p/k\dot{T}(E_p)}-1}$$

or

$$\frac{E_q-E_p}{kT_r}=\frac{E_q}{k\dot{T}_{(E_q)}}-\frac{E_p}{k\dot{T}_{(E_p)}} \tag{17}$$

An interesting result is obtained when the lower energy level is the ground state. Then $E_p = 0$ and Equation 17 reduces to

$$\frac{E_q}{kT_r}=\frac{E_q}{k\dot{T}(E_q)}$$

or

$$T_r=\dot{T}_{(E_q)} \tag{18}$$

It is important to realize that $\dot{T}(E)$ does not represent the weighted average or the average flame temperatures. They are given by

$$T_{average} = \frac{\int_o^{\ell} dx\ T(x)}{\int_o^{\ell} dx}$$

and

$$T_{weighted\ average} = \frac{\int_o^{\ell} dx\ n_o(x)\ T(x)}{\int_o^{\ell} dx\ n_o(x)}$$

Thus, the result of a reversal measurement in a non-isothermal flame, even when self-absorption is negligible, does not have real scientific value because the measurement does not represent the average or weighted average temperatures of the flame. Instead the measured temperature is related to the values of $\dot{T}_{(E_q)}$ and $\dot{T}_{(E_p)}$, and therefore the "reversal temperature" depends on the excitation potentials of the upper and lower energy levels of the transition used for the measurement.

Kadyshevich (20) has, in fact, shown that the average or weighted average flame temperatures are not obtained by reversal measurements. However, Kadyshevich apparently did not derive the appropriate theoretical expressions. He also stated that the reversal temperatures are wavelength dependent and that at long wavelengths the reversal temperature would be equal to the average flame temperature. Equation 17 clearly shows the dependence of the reversal measurement on the upper and lower energy levels of the spectral line used for the determination but not on the wavelength. Also, no

evidence was found to support the claim that reversal temperatures performed at long wavelengths yield the average flame temperature.

Sasaki (19) also performed calculations to illustrate the application of the reversal method to non-isothermal flames. His results showed the dependence of the reversal temperature on the optical depth of the thermometric species in the flame. He found an upper limit of the reversal temperature for an optically thin flame and he derived an expression which can be shown to agree with ours once the definition of $\dot{T}$ is introduced. However, he failed to recognize the dependence of the reversal measurement on the upper and lower energy levels of the spectral line employed for the measurement.

B. Emission-Absorption Method

1. Uniform flame

In this method of temperature measurement the ratio of the flame emission and absorption for an appropriate spectral line is determined experimentally, and this information combined with a knowledge of the brightness temperature of the continuum source allows the calculation of the flame temperature (10-14). In a uniform flame B(em)/B(abs) is given by the ratio of Equations 5 and 6

$$\frac{B(em)}{B(abs)} = \frac{\int_{\Delta\nu_{qp}} d\nu\, B_\nu^b\,(\nu,T_f)\,(1-e^{-K(\nu)\ell})}{\int_{\Delta\nu_{qp}} d\nu\, B_\nu^b\,(\nu,T_b)\,(1-e^{-K(\nu)\ell})}$$

The value of ν is essentially constant over the frequency range, hence it can be set equal to ν_o, the frequency at the center of the spectral line. Consequently,

$$\frac{B(em)}{B(abs)} = \frac{B_\nu^b\,(\nu_o,T_f)}{B_\nu^b\,(\nu_o,T_b)} = \frac{e^{h\nu_o/kT_b}-1}{e^{h\nu_o/kT_f}-1}$$

Clearly, the flame temperature can be determined once the values of B(em)/B(abs) and T_b are known.

In general, the line reversal and the emission-absorption methods are very similar, with the same advantages and disadvantages. The main difference is that the emission-absorption technique is not limited to the maximum brightness temperature of the continuum source. However, the precision and accuracy of the reversal method is much better because it is a null method.

2. Isothermal flame with a non-homogeneous distribution of the thermometric species

The ratio of B(em) and B(abs) given by Equations 10 and 11, integrated over the frequency with $\nu \simeq \nu_o$, yields the same result as for a uniform flame,

$$\frac{B(em)}{B(abs)} = \frac{B_\nu^b\,(\nu_o,T_f)}{B_\nu^b\,(\nu_o,T_b)} = \frac{e^{h\nu_o/kT_b}-1}{e^{h\nu_o/kT_f}-1}$$

Therefore, this method retains its validity for this type of flame.

3. Non-isothermal flame with a non-homogeneous distribution of the thermometric species

As in the reversal method, only the case when self absorption effects are negligible will be considered. Following the thought process employed for developing Equations 12 and 13:

$$\frac{B(em)}{B(abs)} = \frac{\int_o^{\ell} dx\, n_o(x)\, e^{-E_q/kT(x)}}{\left(\frac{1}{e^{E_q-E_p/kT_b}-1}\right) \int_o^{\ell} dx \left(n_o(x) e^{-E_p/kT(x)} - n_o(x) e^{-E_q/kT(x)}\right)}$$

If the definition of $\dot{T}(E)$ is introduced, then

$$\frac{B(em)}{B(abs)} = \frac{e^{E_q-E_p/kT_b} - 1}{e^{E_q/k\dot{T}(E_q) - E_p/k\dot{T}(E_p)} - 1}$$

The actual experimental measurement yields:

$$\frac{B(em)}{B(abs)} = \frac{e^{E_q-E_p/kT_b} - 1}{e^{E_q-E_p/kT_{em-abs}} - 1}$$

where T_{em-abs} is the emission-absorption temperature. Therefore,

$$\frac{E_q-E_p}{kT_{em-abs}} = \frac{E_q}{k\dot{T}(E_q)} - \frac{E_p}{k\dot{T}(E_p)} \qquad (19)$$

Thus, emission-absorption measurements give the same result as reversal measurements for non-isothermal flames. Their dependence on the temperature and concentration gradients in the flame, on the particular spectral line used and on its optical depth explains the variation of infrared emission-absorption temperature measurements in non-isothermal flames observed by Silverman (10) and Tourin and Krakow (27).

C. The Slope Method

1. Uniform flame

The slope method is based on the measurement of integrated line intensities for a number of transitions between different energy levels of the thermometric species in the absence of self absorption effects (11,15-17). When self-absorption is negligible Equation 1 reduces to

$$B(em) = \int_{\Delta\nu_{qp}} d\nu \int_{o}^{\ell} dx \left(\frac{1}{4\pi} A_{qp} h\nu n_q P(\nu) \right)$$

If the integrations are performed with $\nu \simeq \nu_o$, then

$$B(em) = \frac{1}{4\pi} A_{qp} h\nu_o n_q \ell \qquad (20)$$

This expression can be rearranged and the equation for a Boltzmann distribution substituted for n_q. Thus,

$$\ln \left(\frac{g_q A_{qp} \nu_o}{B(em)} \right) = \frac{E_q}{kT_f} + \ln \left(\frac{4\pi g_o}{h\ell n_o} \right) \qquad (21)$$

where n_o and g_o refer to the ground state. A plot of

$\ln(g_q A_{qp} \nu_o / B(em))$ vs. E_q using several spectral lines will yield a straight line with slope equal to $1/kT_f$. The flame temperature is then determined by a measurement of the slope.

The method has the advantage of not having limitations on the applicable temperature range. As only the measurement of the integrated emission intensity of several spectral lines is required, there is no need for any other spectroscopic source than the flame itself. However, a calibration of the response of the spectrometer with respect to wavelength is needed and consequently a calibrated lamp is required. The calibration is usually done at low temperatures where tungsten lamps are quite stable and the same lamp can be used over a long period of time.

On the other hand, there are some conditions which must be satisfied. The emission intensity measurements must not be affected by self-absorption and should be proportional to the integrated line radiances. The spectral calibration factors must also be determined accurately and accurate relative transition probabilities must be available.

2. Isothermal flame with a non-homogeneous distribution of the thermometric species

The expression for B(em) with negligible self-absorption is now given by

$$B(em) = \frac{1}{4\pi} A_{qp} \, h\nu_o \int_o^{\ell} dx \, n_q(x)$$

or

$$B(em) = \frac{1}{4\pi} A_{qp}\, h\nu_o \frac{g_q}{g_o} e^{-E_q/kT_f} \int_o^{\ell} dx\, n_o(x)$$

If the definition of $\overline{n_o}$ is used and the equation rearranged, then the following relationship is obtained,

$$\ln\left(\frac{g_q A_{qp} \nu_o}{B(em)}\right) = E_q/kT_f + \ln\left(\frac{4\pi g_o}{h\ell\overline{n_o}}\right) \qquad (22)$$

The value of the slope will again be $1/kT_f$. Therefore, the slope method retains its validity.

3. Non-isothermal flame with a non-homogeneous distribution of the thermometric species

If the definition of $\dot{T}(E)$ is introduced into Equation 12, then

$$B(em) = \frac{1}{4\pi} A_{qp}\, h\nu_o \frac{g_q}{g_o} e^{-E_q/k\dot{T}(E_q)} \int_o^{\ell} dx\, n_o(x)$$

The integral can be replaced by Equation 9, to yield

$$B(em) = \frac{1}{4\pi} A_{qp}\, h\nu_o \frac{g_q}{g_o} e^{-E_q/k\dot{T}(E_q)}\, \overline{n_o}\, \ell$$

and after rearranging,

$$\ln\left(\frac{g_q A_{qp} \nu_o}{B(em)}\right) = \frac{E_q}{k\dot{T}_{(E_q)}} + \ln\left(\frac{4\pi g_o}{h\ell\overline{n_o}}\right) \qquad (23)$$

This expression is very similar to Equations 21 and 22, but now the plot may not produce a straight line because the value of $\dot{T}_{(E_q)}$, being a function of the excitation potential, is not constant. It will be shown later that when the flame

is not far from being isothermal and the range of excitation potentials is not too large, a reasonable straight line is obtained. However, even in this case, the value measured is $\dot{T}$ for this excitation potential range, and $\dot{T}$ may be quite different than the average flame temperature. Therefore, for a non-isothermal flame, the slope method may not produce a straight line, and even when it does the slope will not yield the average flame temperature but rather the value of $\dot{T}$ in the range of excitation potentials employed. The actual expression for the "slope temperature" is given by equating the slope of the plot based on Equation 23 to $1/kT_{slope}$, as previously done for isothermal flames. Thus, at a given value of the excitation potential E_q,

$$\frac{\partial}{\partial E_q}\left(\frac{E_q}{k\dot{T}_{(E_q)}}\right) = \frac{1}{kT_{slope(E_q)}}$$

In the Appendix A this equation is shown to yield

$$\frac{1}{kT_{slope}} = \frac{\int_o^{\ell} dx\, n_o(x)\, \frac{1}{T_{(x)}}\, e^{-E_q/kT(x)}}{\int_o^{\ell} dx\, n_o(x)\, e^{-E_q/kT(x)}} \qquad (24)$$

This equation agrees with the expression previously derived, in a different way, by Desai and Corcoran (24).

D. The Two Line Method

1. Uniform flame

The two line method is really a special case of the slope method when the measurements are limited to two spectral lines (2,18). There is no need to have a temperature plot since from Equation 21 the following relationship is obtained

$$\ln\left(\frac{g_q A_{qp} \nu_o}{B(em)}\right) - \ln\left(\frac{g_{q'} A_{q'p'} \nu'_o}{B'(em)}\right) = \frac{E_q - E_{q'}}{kT_f} \qquad (25)$$

Thus, the flame temperature can be calculated by the use of Equation 25. Although the use of only two lines to determine the flame temperature is simpler and faster than the use of several lines as required by the slope method, the uncertainties in the result are larger because a small error in the intensity measurement or in the transition probability for one of the lines will greatly influence the calculated value for the flame temperature.

2. Isothermal flame with a non-homogeneous distribution of the thermometric species

Equation 22 may be used to derive an expression identical to Equation 25. Therefore, the two line method gives again the value of the flame temperature.

3. Non-isothermal flame with a non-homogeneous distribution of the thermometric species

When applied to only two spectral lines, Equation 23

becomes

$$\ln\left(\frac{g_q A_{qp} \nu_o}{B(em)}\right) - \ln\left(\frac{g_{q'} A_{q'p'} \nu_o}{B'(em)}\right) = \frac{E_q}{k\dot{T}_{(E_q)}} - \frac{E_{q'}}{k\dot{T}_{(E_{q'})}}$$

The "Two line temperature" is given then, by

$$\frac{E_q - E_{q'}}{kT_{\text{two line}}} = \frac{E_q}{k\dot{T}_{(E_q)}} - \frac{E_{q'}}{k\dot{T}_{(E_{q'})}} \qquad (26)$$

If Equations 27 and 26 are compared, it is seen that the reversal and two-line techniques yield the same results if the excitation potentials of the spectral lines observed for the two-line method correspond to the upper and lower energy levels of the transition used for the reversal determination. Again, the result of the measurement is not the average flame temperature. Obviously, $E_{q'}$ can never be equal to zero as in the reversal measurement (see Equation 18) so the value of $\dot{T}$ at some value of the energy cannot be measured by this method.

E. Conclusion

The theoretical discussions above have clearly shown that spectroscopic temperatures measurements of non-isothermal, non-homogeneous flames by the line reversal, emission-absorption, slope, or two-line methods, when self-absorption effects are negligible, yield results which depend on: (a) the measurement method employed; (b) the energy of the quantum states involved in the line producing transition(s); (c) the particu-

lar flame temperature gradient prevailing in the flame; and (d) the concentration distribution of the thermometric species. It was also emphasized that the results at these temperature measurements do not represent the average (T_{ave}) or weighted temperature average ($T_{w.a.}$) of the flame. Since a range of energy states may typically be involved in measurements on flames possessing a variety of temperature gradients and concentration distributions of the thermometric species, it is of interest to inquire how these factors affect the degree of divergence of the measured temperatures from $T_{(ave)}$ or $T_{(w.a.)}$. These evaluations may be accomplished by generating sets of logical temperature gradients and concentration profiles of the thermometric species and solving the appropriate equations. These evaluations, to be presented in detail in a subsequent section, will show that the measured temperatures may diverge as much as 200 to 500°K from $T_{(ave)}$ or $T_{(w.a.)}$ - a degree of divergence which really is intolerable if the temperatures are to be used for definitive calculations of interesting flame equilibria and processes.

IV. FLAME MODEL CALCULATIONS

Several temperature and concentration profiles were generated by the use of the following equations:

$$T(x) = 500 + 2500 \cos\left(\frac{\pi x}{2d}\right)\left(\frac{e^{-\alpha(x/d)^2}}{N(\alpha)}\right) \qquad (27)$$

$$n_o(x) = 1 + 999 \cos\left(\frac{\pi x}{2d}\right)\left(\frac{e^{-\beta(x/d)^2}}{N(\beta)}\right) \qquad (28)$$

where $d = \ell/2$ and ℓ is the length of the optical path, x assumes values from +d to -d, α and β are parameters which characterize each profile and $N(\alpha)$ and $N(\beta)$ are normalizing parameters so that $e^{-\alpha(x/d)^2} \leq 1$ (the same for β). There is no need to know absolute values of the concentration of the thermometric species in the ground state because $\dot{T}_{(E)}$ depends only on the relative distribution of $n_o(x)$ (see Equations 15 and 16). The maximum and minimum value of the temperature (3000°K and 500°K) and the ratio of the maximum and minimum values of n_o (1000:1) are the same for all the profiles. These equations are similar to the ones used by Sasaki (19) to generate temperature and concentration distributions.

Figure 1 shows 4 temperature profiles which correspond to the values of α = 0, 2, -1 and -5. These temperature profiles combined with identical (β = 0, 2, -1 and -5) concentration profiles provided 16 different theoretical flame models used in this study. Figures 2, 3 and 4 show the computer calculated

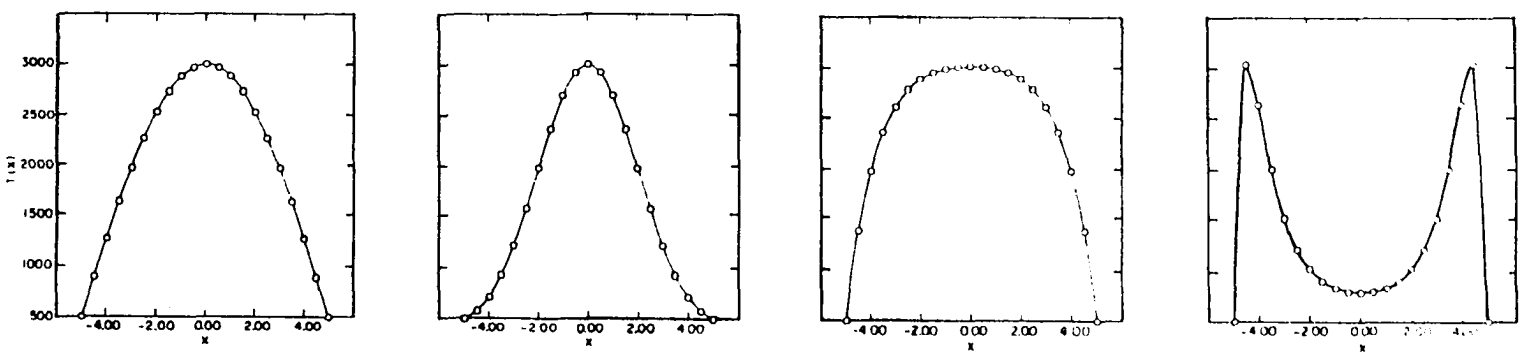

Fig. 1. Temperature profiles

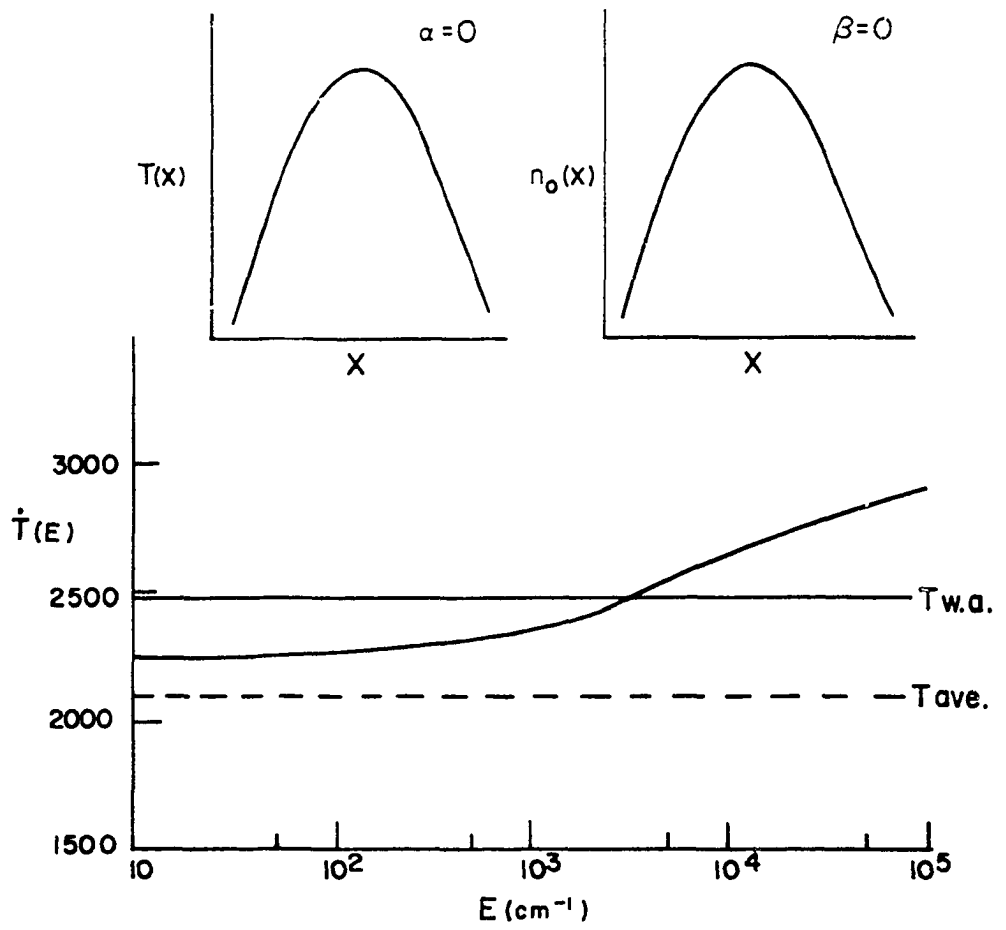

Fig. 2. Calculated $\dot{T}_{(E)}$, $T_{ave.}$ and $T_{w.a.}$ (in Kelvins) for $\alpha = 0$ and $\beta = 0$ profiles

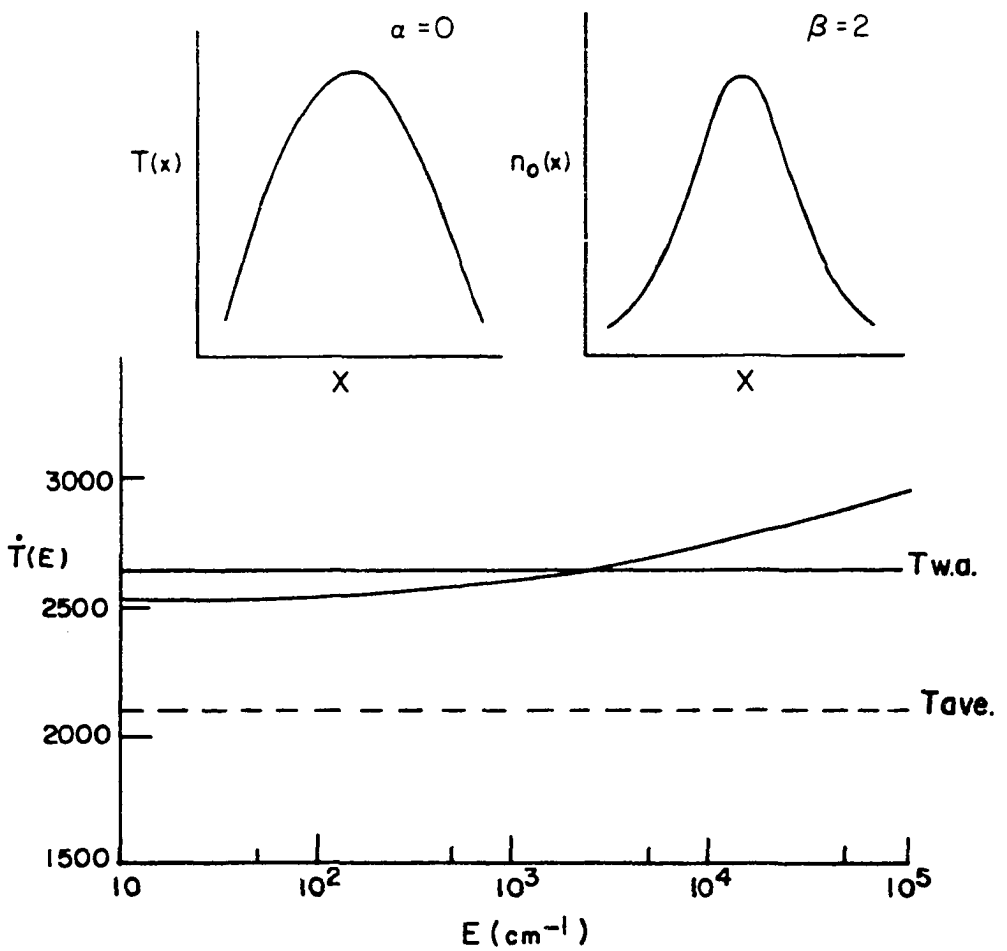

Fig. 3. Calculated $\dot{T}_{(E)}$, $T_{ave.}$ and $T_{w.a.}$ (in Kelvins) for $\alpha = 0$ and $\beta = 2$ profiles

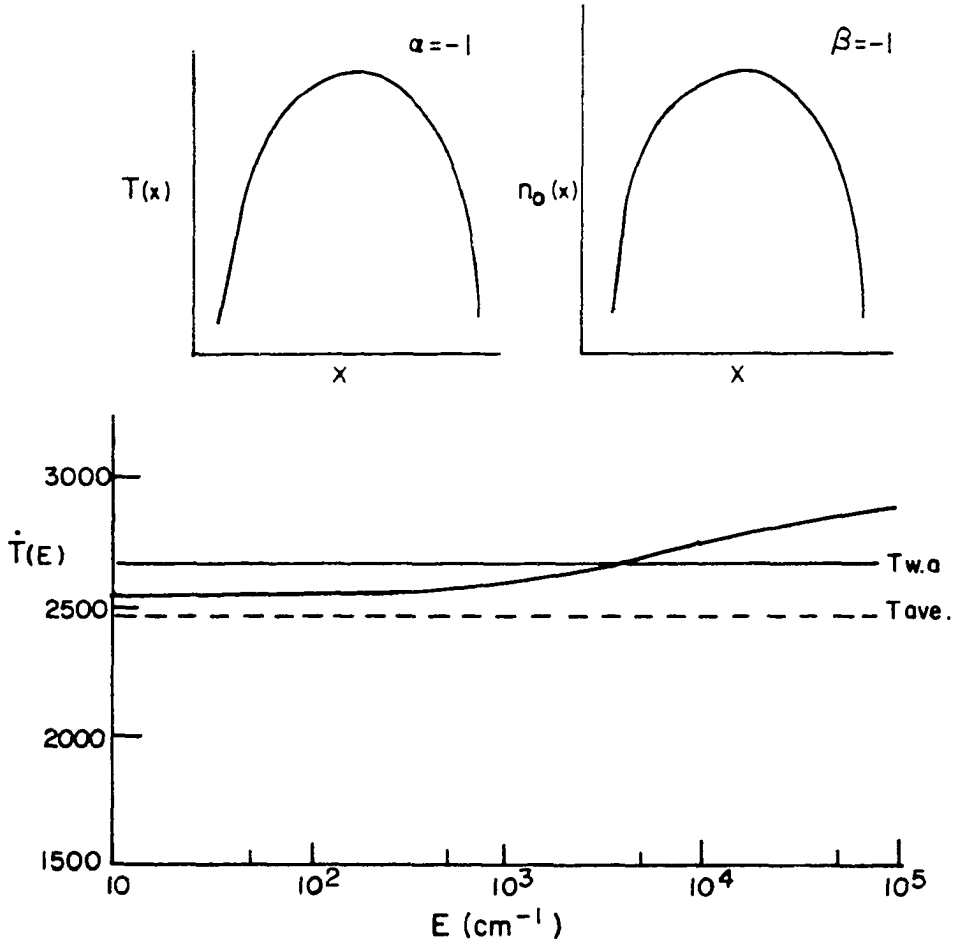

Fig. 4. Calculated $\dot{T}_{(E)}$, $T_{ave.}$ and $T_{w.a.}$ (in Kelvins) for $\alpha = -1$ and $\beta = -1$ profiles

values of $\dot{T}_{(E)}$ at different values of the atomic energy states E for 3 realistic flame models. Similar results were found for all the combinations of temperature and concentration profiles. The value of $\dot{T}_{(E)}$ was calculated by means of the equation

$$e^{-E/k\dot{T}(E)} = \frac{\int_o^{\ell} dx\ n_o(x)\ e^{-E/kT(x)}}{\int_o^{\ell} dx\ n_o(x)} \tag{29}$$

The T(x) and $n_o(x)$ terms were generated from Equations 27 and 28 respectively. The average and weighted average temperatures, also indicated in the figures, were calculated using the following relationships:

$$T_{ave.} = \frac{\int_o^{\ell} dx\ T(x)}{\int_o^{\ell} dx}$$

and

$$T_{w.a.} = \frac{\int_o^{\ell} dx\ n_o(x)\ T(x)}{\int_o^{\ell} dx\ n_o(x)}$$

It is of interest to note that the value $\dot{T}_{(E)}$ assumes special significance at three levels of the energy. (1) In the limit as $E \to 0$, Equation 29 can be approximated by

$$1 - \frac{E}{k\dot{T}_{(E)}} = 1 - \frac{E}{k}\ \frac{\int_o^{\ell} dx\ n_o(x)\ \frac{1}{T(x)}}{\int_o^{\ell} dx\ n_o(x)}$$

simplifying,

$$\frac{E}{k\dot{T}_{(E)}} = \frac{E}{k}\left(\frac{\overline{1}}{T}\right)$$

or

$$\frac{1}{\dot{T}_{(E)}} = \left(\frac{\overline{1}}{T}\right)$$

Thus, at very low values of the energy, $\dot{T}_{(E)}$ is given by $1/(\overline{1/T})$, where $(\overline{1/T})$ is the weighted average of $1/T(x)$ over the optical path. (2) At high values of the energy E (around 100,000 cm^{-1}) $\dot{T}_{(E)}$ approaches the maximum flame temperature because the only significant contributions to $\dot{T}_{(E)}$, i.e. the only significant values of $e^{-E/kT(x)}$ in Equation 29, arise from the highest temperature region. (3) Inspection of Figures 2 to 4 shows that the value of $\dot{T}_{(E)}$ at $E \simeq 3000$ cm^{-1} is the same as the weighted average value of the flame temperature for the flame models and boundary conditions specified above. No proof has been found that this result can be generalized for all temperature and concentration profiles, and boundary conditions for these profiles.

The significance and implications of the data plotted in Figures 2, 3 and 4 will be examined in some detail. At the top of Tables 2, 3 and 4 are shown the calculated $T_{ave.}$ and $T_{w.a.}$ for a flame possessing either an $\alpha = 0$ or $\alpha = 1$ temperature profile, with $T_{max} = 3000^{o}K$ and $T_{min} = 500^{o}K$ as boundary conditions and for either a $\beta = 0$, $\beta = 2$, or $\beta = -1$ thermo-

Table 2. Computer calculated temperatures for a flame model characterized by a $\alpha = 0$ temperature distribution and a $\beta = 0$ concentration distribution

$\alpha = 0$	$\beta = 0$
$T_{average} = 2092$	T weighted average = 2463
$E_q - E_p$ (cm^{-1})	"Temperature"
40,000 - 0	2821
30,000 - 0	2788
20,000 - 0	2737
10,000 - 0	2638
40,000 - 30,000	2925
30,000 - 20,000	2896
20,000 - 10,000	2844

Table 3. Computer calculated temperatures in a flame model characterized by a $\alpha = 0$ temperature distribution and a $\beta = 2$ concentration distribution

$\alpha = 0$	$\beta = 2$
$T_{average} = 2092$	T weighted average = 2640
$E_q - E_p$ (cm^{-1})	"Temperature"
40,000 - 0	2858
30,000 - 0	2835
20,000 - 0	2800
10,000 - 0	2736
40,000 - 30,000	2929
30,000 - 20,000	2908
20,000 - 10,000	2867

Table 4. Computer calculated temperatures in a flame model characterized by a $\alpha = -1$ temperature distribution and a $\beta = -1$ concentration distribution

$\alpha = -1$	$\beta = -1$
$T_{average} = 2469$	T weighted average = 2683
$E_q - E_p$ (cm^{-1})	"Temperature"
40,000 - 0	2882
30,000 - 0	2863
20,000 - 0	2833
10,000 - 0	2776
40,000 - 30,000	2941
30,000 - 20,000	2925
20,000 - 10,000	2892

metric species concentration profile, with n_o max = 1000 and n_o min = 1 as boundary conditions. The remainder of the tables show "temperatures" calculated in accordance with Equations 17, 19 and 26 (which are in fact identical) for the line reversal, emission-absorption and two-line method. These temperatures would be determined if the measurements were made under conditions of negligible self-absorption and no systematic errors were involved. It should be noted that in Tables 2, 3 and 4, q and p denote, for reversal and emission-absorption measurements, the upper and lower energy levels of the transition used in the determination. For the two-line method, q and p refer to the upper energy levels of the two spectral lines employed in the measurement. If the concentration of the radiating species is increased until self-absorption is

no longer negligible, then the value of the reversal and emission-absorption temperatures will be lower, as illustrated by Sasaki (19) for reversal measurements. According to Kadyshevich (20) the average flame temperature would result from line reversal measurements at large wavelengths and at small concentrations of the radiating species. The calculations discussed above do not support this conclusion.

Calculations by Desai and Corcoran (24) for plasmas and Hefferlin and Gearhart (21) for arcs have shown that the slope method yields a straight line even in a non-isothermal temperature source. The results obtained in this work for all the different flame models are in agreement with this conclusion. For example, Figure 5 shows the temperature plot for the $\alpha = 0$, $\beta = 0$ flame model in the energy range from 10,000 cm^{-1} to 50,000 cm^{-1}. The actual change of the slope is less than 3% and consequently no curvature is present to identify the flame as non-isothermal.

Thus, it has been clearly shown that spectroscopic temperature measurements of non-isothermal flames by the reversal, emission-absorption, slope and two-line techniques cannot lead to temperature values which have physical significance in an exact sense. The "temperature" values obtained by these techniques differ by several hundred degrees from the average or weighted average flame temperatures. Moreover, temperature measurements by the same technique but with different spectral

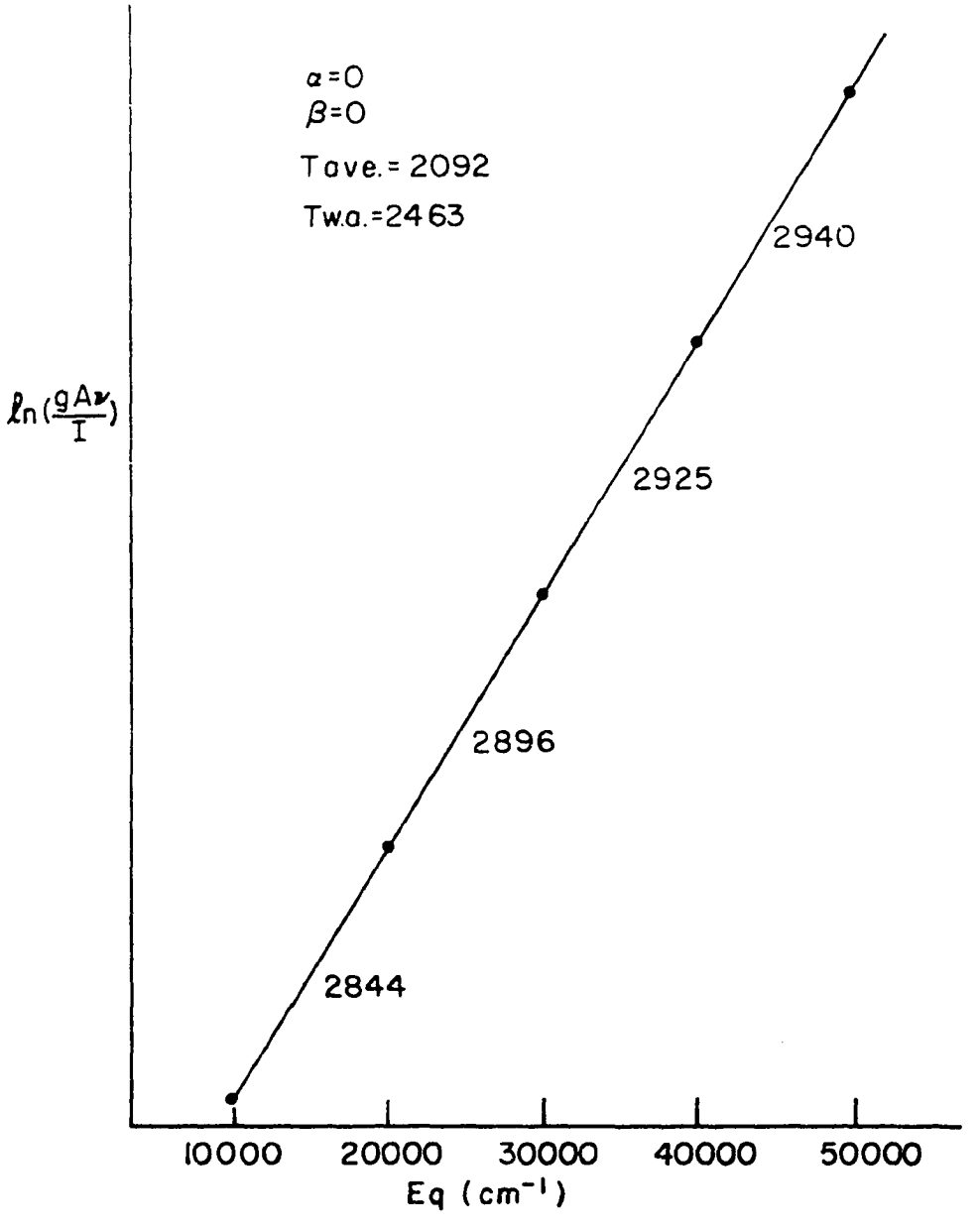

Fig. 5. Slope temperature plot for α = 0 and β = 0 profiles. Temperatures are in Kelvins

lines differ by as much as 200°K. Therefore, any interpretation that goes beyond the uncertainties illustrated in Figures 2 to 4 and Tables 2, 3 and 4 simply flatters the actual experimental situation. As these uncertainties can be as high as 900°K, it is doubtful that temperature measurements in non-isothermal flames can be of definitive scientific value.

Since real flames are not isothermal, spectroscopic flame temperature measurements are then useful only if (a) the thermometric species resides only in an isothermal temperature field; or (b) if Abel inversion techniques are employed to transform the experimentally determined lateral distribution of the spectral line radiances to their corresponding radial distributions.

Isothermal temperature fields may be obtained in shielded flames (37-40), in which the thermometric species is introduced exclusively into the central part of the flame and consequently protected from the temperature gradients at the edges, or in flames in which the chemical environment isolates the thermometric species to the central part of the flame, as in the interconal zone of fuel rich nitrous oxide or oxyacetylene flames (41,42). It is also possible to obtain a practically isothermal temperature field in flames characterized by a long optical path, where the contributions from the flame edges are relatively small. Spectroscopic temper-

ature measurements in flames of the latter type will be discussed in more detail in the next section.

The Abel inversion techniques, its application to the unraveling of non-isothermal temperature profiles for both symmetrical and asymmetrical sources, and the errors involved in the unraveling process have been described in several excellent articles (43-46).

V. EXISTENCE OF ISOTHERMAL TEMPERATURE FIELDS IN SOME FLAMES

The theoretical concepts developed above have shown that if the reversal temperatures measured in a flame are not dependent on: (a) the value of the upper and lower energy levels involved in the line producing transition; and (b) on the optical depth, then, the flame behaves as and may be considered isothermal and the temperature value measured will have physical significance. Actually, these considerations apply only to the flame region where the thermometric species exist. The observation of another thermometric species, which may occupy a different flame region, may not lead to the same results.

Since there are no known flames that can be considered isothermal, it is important to inquire how closely the condition of isothermality for a specific thermometric species may be achieved in a given flame. The demonstrations that isothermal fields may be achieved in a flame would then allow the determination of useful physical parameters such as transition probabilities, optical cross-sections, dissociation energies, which otherwise could not be measured because a homogeneous temperature field, with an accurately known temperature, is needed. These isothermal environments have been obtained by the use of shielded flames in which the thermometric species is introduced only into the inner section of the flame. In this way, the temperature gradients at the flame edges do not affect the measurements (37-40). There

have also been scattered observations in our laboratories that isothermal temperature fields are closely approximated by certain flame systems formed by the combustion of nearly laminar flows of premixed gases on extended slot burners. Flames formed under these conditions possess a long optical path so that contributions from the temperature and thermometric species concentration gradients of the ends of the flame are minimized.

The remarkable growth in the analytical applications of flame atomic absorption spectroscopy and flame atomic emission spectroscopy has stimulated the development of several excellent flame-burner systems of this type. Since all of these burners were specifically designed for the safe introduction of metal additives with the fuel-oxidant mixture, it is a very simple matter to inject selected metallic thermometric species into the inner axial channel of these flames. The degree of isothermality achieved under these conditions may be experimentally determined by simply noting whether variations in the optical depth or in the excitation energies of the upper and lower energy levels involved in the line producing transitions affect the reversal temperature measurements. The results of this experimental study are discussed below.

A. Selection of Flame and Burner

The extensive use of N_2O-C_2H_2 flames as absorption cells for atomic absorption spectroscopy and as emission excitation sources for emission spectroscopy has led to the design of slot-type burner systems which form exceptionally stable flames with long optical paths possessing the characteristics discussed above. The specific burner selected for this study has been described in detail (47). The operating conditions for this burner are listed in Table 4.

B. Selection of Thermometric Species and Spectral Lines

Iron was selected as the thermometric species because: (a) its spectrum is formed by a large number of lines which facilitates the selection of the best ones for this study and (b) if an isothermal temperature field could, in fact, be demonstrated for iron atoms in this flame-burner system, then this system would provide an excellent opportunity to measure accurate relative transition probabilities for iron, which are needed for accurate temperature measurements by the slope and two-line methods.

A selection of iron spectral lines generated by properly separated upper and/or lower energy levels and also capable of providing a high optical depth at the flame had to be made. The last requirement was necessary in order to perform accurate reversal temperature measurements, because this technique is not very sensitive at low optical depths, and to

provide a wide range of optical depths to check for reversal temperature variations.

Since solution concentrations greater than one weight percent tend to interfere with the proper functioning of the nebulizer-burner system, the lines selected must exhibit the desired optical depth at or below this concentration level. The characteristics discussed above were adequately provided by the three iron lines identified in Table 5.

Table 5. Lines used for the study of the Fe temperature field and calculated reversal temperatures for different flame models

(Å)	Energy levels (cm^{-1})	Temperatures (K)		
		$\alpha=0,\beta=0$	$\alpha=0,\beta=2$	$\alpha=-1,\beta=-1$
3719.94	26875 - 0	2777	2826	2855
3734.87	33695 - 6928	2865	2884	2905
3737.13	27167 - 416	2786	2831	2861

To illustrate the differences in reversal temperatures which would be measured with these three iron lines for typical non-isothermal flames under conditions of negligible self-absorption, calculations were performed by means of Equation 17 and the data shown in Figures 2, 3 and 4. The results are also shown in Table 5. It is important to note that the temperatures which would be measured by these three

lines differ as much as 89°K for the (α=0, β=0) model down to a difference of 50°K for the flame model (α=-1, β=-1), which is not far from being isothermal.

C. Experimental Facilities and Procedures

1. Apparatus

The slot burner and the optical and electronic arrangement employed in this study are shown in Figures 6 and 7. The experimental facilities and operating conditions are summarized in Table 6.

The optical arrangement for the temperature measurements was set up to give a 1:1 image of the tungsten lamp and the flame on the spectrometer entrance slit. The entrance slit was restricted to a height of 1 mm. Under these conditions, the volume of gases observed consisted of slightly distorted cones with apexes at the center of the flame and with bases of approximately 7 mm in cross section at the edges of the flame. Thus, the optical measurements were restricted to a small cross section of the long flame. The burner provided an optical path of 76 mm.

2. Techniques

The reversal measurements were accomplished by parking the spectrometer on the spectral line of interest and adjusting the lamp current until no changes in intensity were observed when the thermometric species was nebulized into the

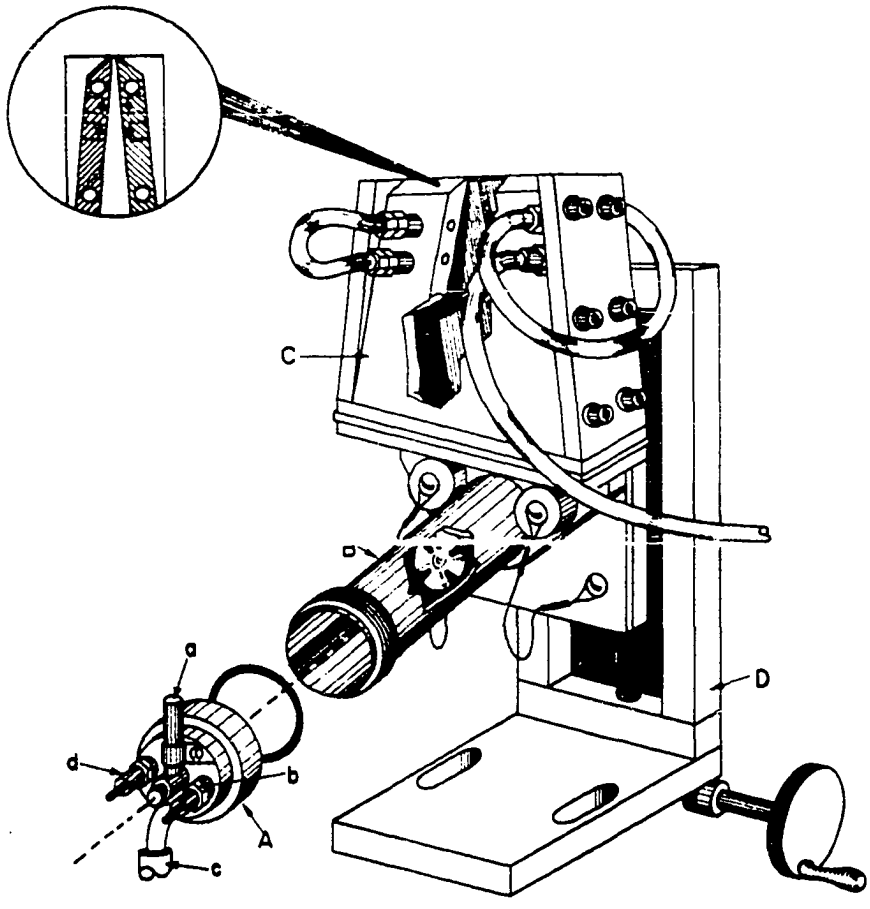

Fig. 6. Cutaway view of long-path slot burner
(A) End-cap assembly showing (a) nebulizer; (b) and (d) fuel port and auxiliary oxidant port; (c) drain pipe
(B) Spray-premixing chamber showing flow spoiler and blow-out plugs
(C) Burner head showing tapered walls and cooling ducts
(D) Burner racking assembly

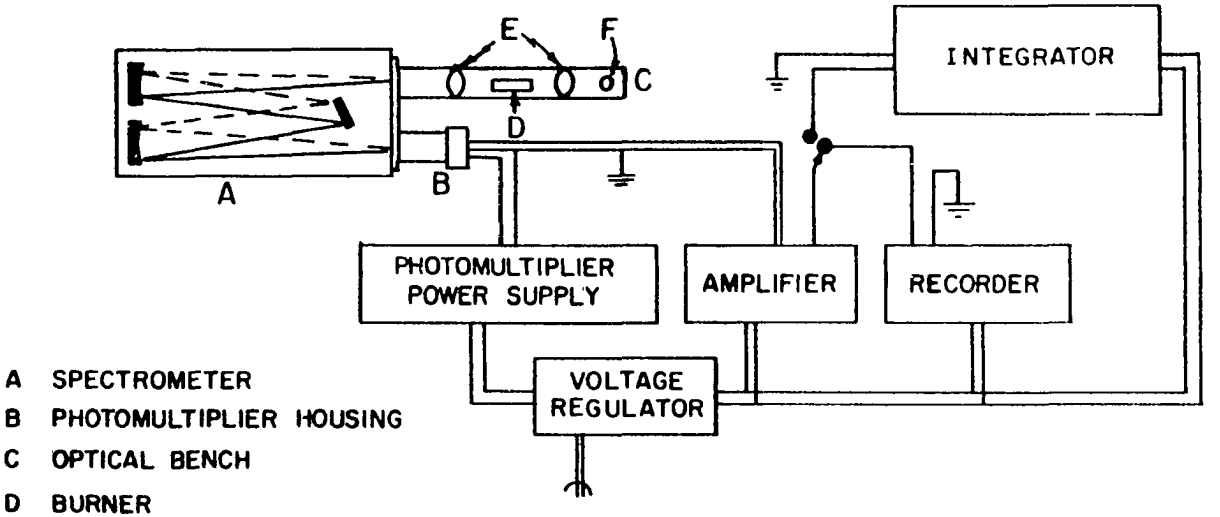

Fig. 7. Block diagram of optical and experimental system

Table 6. Experimental facilities and operating conditions

Burner	Long path, slot burner (47). Slot width 0.25 mm
Flame Gases	Nitrous oxide 12.05 ℓ/min; acetylene 5.40 ℓ/min
Nebulizer input	3.75 ml/min
External optics	5 cms diameter, plane convex, quartz lenses. 16.0 and 10.8 cms focal lengths at 5460Å. The optical arrangement was set up to give a 1:1 image of the flame and tungsten lamp on the spectrometer entrance slit
Spectrometer	1.0 m Czerny Turner mount Jarrell Ash Model 78-462 scanning spectrometer. Effective aperture, f/8.7. 1180 grooves/mm grating blazed for 2500Å. R.l.d. 8.2 Å/mm in the first order
Detector	EMI 6256B Photomultiplier. Spectral response type, 513. Approximate useful sensitivity range, 1650Å-6500Å
Detector power supply	Model S-325-RM, New Jersey Electronic Corporation (500-2500v, 0-10 mA).
Amplifier	Leeds and Northrup 9836-B microammeter
Recorder	Leeds and Northrup Speedomax G Model S millivolt recorder
Voltage regulator	Superior Electric Company 1 KVA Stabiline automatic voltage regulator Model 1G5 101
Readout System	Infotronics Corp., Model CRS-80 Digital Readout System, Series No. 3564. Meas. interval (sec.) 12, Mode Linear.
Primary source	Westinghouse type EDW-6V, 18A, tungsten strip filament lamp
Pyrometer	8641 Mark I Precision Automatic Optical Pyrometer. Leeds and Northrup Company. Specially calibrated with estimated uncertainties of less than $\pm$ 7°K in the temperature range used (2000-3000°K)

flame. The reversal points were then related to the reversal temperatures through the brightness temperature calibration of the lamp.

The lamp calibrations were determined as follows. Temperature measurements were first performed on tungsten strip lamps at several current levels by means of an accurately calibrated optical pyrometer (see Table 6). This pyrometer had an estimated uncertainty in its calibration of less than $\pm$ 7°K in the temperature range used (2000-3000°K). Since the pyrometer measured the brightness temperature of the lamp at 6450Å, the actual temperature of the tungsten filament was calculated by means of the following equation, which is obtained by the use of Wien's law and the definition of the brightness temperature,

$$e^{-c_2/\lambda T_b} = \varepsilon(\lambda,T)\ \tau_g(\lambda)\ e^{-c_2/\lambda T} \qquad (30)$$

where c_2 is the second radiation constant which is equal to 0.014388 according to the International Practical Temperature Scale of 1968, $\varepsilon(\lambda,T)$ is the emissivity of tungsten, $\tau_g(\lambda)$ is the transmission of the glass envelope of the lamp, T is the temperature of the tungsten strip and λ is the wavelength at which the calibration measurement was performed (6450Å). The values of $\varepsilon(\lambda,T)$ were taken from de Vos (48) and the transmissions of the glass envelopes were measured in the laboratory.

The temperature of the tungsten filament at the reversal point was used to calculate the reversal temperature of the flame, i.e. the brightness temperature of the lamp at the flame and at the wavelength of the reversal measurement, by means of Equation 31 (similar to Equation 30):

$$e^{-c_2/\lambda T_b} = \epsilon(\lambda,T)\ \tau_g(\lambda)\ \tau_\ell(\lambda)\ e^{-c_2/\lambda T} \qquad (31)$$

where $\tau_\ell(\lambda)$ is the transmission of the lens used to focus the lamp on the flame.

Considerable care was taken to assure the accuracy of the reversal measurements. The angle of acceptance of the spectrometer was used as the limiting aperture and was completely filled by the continuum radiation from the calibrated lamp. A diaphragm was placed in front of the flame to reduce the incidence of stray light from the flame into the spectrometer. The same area of the tungsten strip filament used for calibration purposes was also used for reversal measurements. The precision obtained with the system was less than $10^{\circ}K$.

D. Results and Discussion

It should be indicated that this study is based essentially on the observations of changes in reversal temperature measurements rather than in the determination of absolute temperature values. The experimental data collected showed that neither the value of the energy levels of the spectral lines nor the concentration of the thermometric species (over a

20-fold range) affected the reversal temperature measurements beyond the experimental error of 10°K. Also, no changes in the temperatures were found when the lens closest to the spectrometer was masked to a diameter of only 3 mm, restricting the optical measurements to an even smaller cross section of the central part of the flame.

Thus the Fe atoms indeed behaved as if they occupied an isothermal temperature field. The experimental data do not provide any definitive insight on the spatial distributions of the Fe atoms because as shown earlier in this thesis, reversal temperature measurements on a thermometric species which occupies an isothermal temperature field are not affected by concentration gradients in that field.

The demonstration that the Fe atoms do reside in an isothermal temperature field in this flame presents an excellent opportunity to employ this system for the precise measurement of some fundamental and useful physical properties of Fe. The determination of one of these properties - the accurate relative transition probabilities for Fe spectral lines - will be discussed in the remainder of this thesis.

VI. PRESENT STATE OF KNOWLEDGE OF Fe ATOMIC TRANSITION PROBABILITIES

The accuracy of temperature measurements by either the slope or two-line methods is directly dependent on the accuracy of transition probability data for the line producing transitions. Accurate values for these fundamental properties of atoms are also essential in calculations of theoretical line profiles, for the quantitative assay of stellar atmospheres, and for many other investigations.

Transition probabilities may be calculated from the wavefunctions of the upper and lower energy states involved in the transition. Except for the simplest atoms, the required wavefunctions are not well known and the values calculated from them are not reliable. Therefore, experimentally determined values are highly desirable, particularly for lines in complex spectra.

The increasing interest in the field is well shown by the number of references given by N.B.S. compilations (49-51): approximately 600 papers published before 1962, 300 more by the beginning of 1966, and even 250 more by the end of 1967. Despite this effort, there are still large disagreements among published absolute transition probabilities. For spectroscopic temperature measurements, relative atomic transition probability values suffice, but even here there are intolerable differences in published values.

The observation that the Fe atoms released in a premixed N_2O-C_2H_2 flame burning on a long path, slot burner occupy a practically uniform temperature field, provided the opportunity to assess the importance of accurate relative transition probability data for precise temperature measurements. This assessment was based on the comparison of slope temperature values obtained for two groups of iron lines with the use of several sets of transition probability values published in the literature.

A. Requirements for Accurate Temperature Measurements by the Slope Method

In addition to the availability of accurate relative atomic transition probability data, several additional important experimental conditions must be satisfied. These requirements have not been generally recognized or fulfilled in many temperature measurements described in the published literature. First, integrated line radiances or quantities strictly proportional to these radiances must be measured. As it is well known, when the spectrometer is set at a given wavelength, the response obtained is not the spectral radiance at that particular wavelength but rather a sum of contributions from a given wavelength interval called the band pass of the instrument. The weight of each contribution determines a curve called the slit function (52). Slit function consid-

erations indicate that 3 different procedures may be used to measure integrated line radiances. The first one involves scanning the line and measuring the area under the curve. The result is independent of the slit function of the instrument (7). The second procedure is based on using equal but very large entrance and exit slits, much larger than the line width, so that the slit function remains essentially constant in the wavelength region occupied by the line (7). In the third procedure exit slits larger than the entrance slit are used. Under these conditions, the image of the entrance slit falls entirely within the exit slit aperture and the signal detected, i.e. the measured intensity, is then proportional to the integrated line radiance. For the temperature determinations described below, the third procedure was used exclusively because the measurements are relatively simple and it is easy to verify that the experimental requirements are met. When the exit slit is sufficiently larger than the entrance slit, a scan of the spectral line should produce a trapezoidal line shape, as shown in Figure 8 (52). A proper combination of entrance and exit slits should yield a trapezoidal line shape for all the spectral lines of interest. Under these conditions, the photocurrent level observed at any point between a and b in Figure 8 constitutes the desired signal, which is proportional to the integrated line radiance. However, some problems may arise if the photomultiplier response

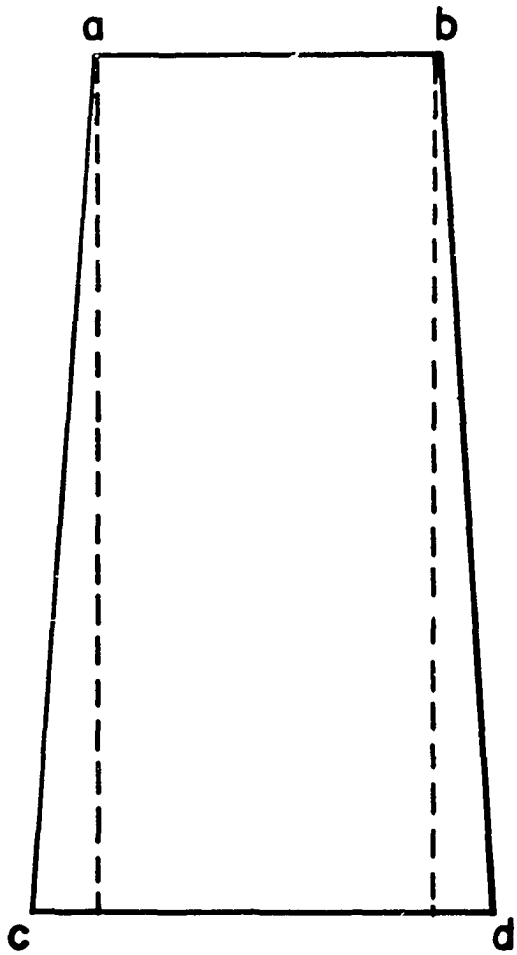

Fig. 8. Characteristic line shape or strip chart profile with the exit slit longer than the entrance slit

is not constant across the bandpass of the spectrometer. This situation was encountered in this research work and the problems involved were illustrated in a recent publication (53).

When the exit slit of the spectrometer is larger than the entrance slit, the measured signals or line intensities can be shown to be equal to

$$I^{meas}_{(em)} = C(\nu)\ B(em) \tag{32}$$

where

$$C(\nu) = \frac{I^{meas}_{(cont)}}{\Delta\nu\ B^{b}_{\nu}(\nu_o, T_b)} \tag{33}$$

$I^{meas}_{(em)}$ is the measured line intensity, $I^{meas}_{(cont)}$ is the signal detected when a calibrated tungsten lamp at a brightness temperature T_b is focused on the spectrometer entrance slit, $\Delta\nu$ is the bandpass of the instrument and $C(\nu)$ is the spectrometer calibration factor. These equations are derived in Appendix B.

The spectrometer calibration factors were determined by means of tungsten lamp strips calibrated at our laboratory with a very accurate optical pyrometer. The bandpass of the instrument, at several wavelengths, was measured by scanning a spectral line and dividing the area under the curve by the peak intensity (see Appendix B).

Assurance must also be provided that the measured inte-

grated line radiances are not affected by self-absorption effects. This assurance may most conveniently and decisively be obtained from "curve of growth" plots, which are plots of the logarithm of the integrated radiance of a spectral line vs. the logarithm of the optical depth (36). These curves are obtained experimentally by plotting the logarithm of the measured integrated line intensity vs. the logarithm of the solution concentration. Growth curves show several important features as illustrated in Figure 9. For low concentrations they follow a straight line of slope equal to one and for high concentrations a straight line with slope equal to 1/2. The form of the curve between these two regions depends on the particular line shape. The slope = 1 region corresponds to the range of optical depths, i.e. solution concentrations, for which self-absorption effects are negligible. Thus, if curve of growth data are collected for all of the lines of interest, the concentration levels corresponding to negligible self-absorption and maximal signal to noise ratios may be selected. In this way, different concentrations may have to be used for different spectral lines. However, in order to produce the temperature plot Equation 21 requires a single value of n_o, i.e. solution concentration, for all the spectral lines. Since self-absorption is absent, the measured integrated line intensities are directly proportional to the solution concentrations. Therefore, all the measured line

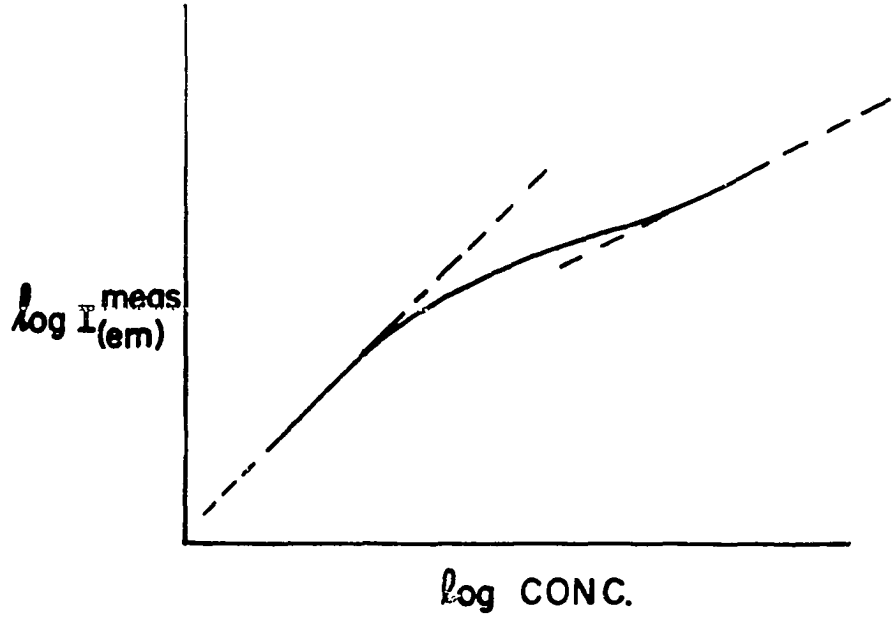

Fig. 9. Curve of growth

intensities can be easily normalized to a single solution concentration.

B. Selection of Groups of Fe Lines

The groups of Fe lines for observation were selected with care. Among the factors considered in the selection process were: (a) freedom of spectral interference from flame components; (b) maximal spread in excitation potentials to minimize the relative error in the measurement of the slope of the temperature plot; (c) sufficient spectral intensity so that the solution concentrations required fell within the operating limits of the nebulizer-burner system; and (d) wavelength proximity, to avoid adjustments in the external optical system arising from the wavelength dependence of the focal length of the lenses.

The primary set of nine Fe lines is shown in Table 7. A secondary set of eight lines was assembled to serve primarily as a consistency check on the primary set. For the selection of lines in the secondary set, attention was also focused on their proclivity toward self-absorption. This selection was not done as a check on the freedom of self-absorption under the experimental conditions employed in this study because this assurance was derived from curve of growth evolutions. Rather, the secondary set of lines should have been less subject to systematic errors from self-absorption

effects when their translation probabilities were measured by other investigators. The secondary set of lines is shown in Table 8; some of the lines in the primary set are included in the secondary group.

Table 7. Nine line set

Wavelength (Å)	Energy levels (cm^{-1})
3608.86	35856 - 8155
3618.77	35612 - 7986
3631.46	35257 - 7728
3647.84	34782 - 7377
3679.92	27167 - 0
3705.57	27395 - 416
3899.71	26340 - 704
3922.91	25900 - 416
3930.30	26140 - 704

Table 8. Eight line set

Wavelength (Å)	Energy levels (cm^{-1})
3476.70	29733 - 978
3497.84	29469 - 888
3608.86	35856 - 8155
3618.77	35612 - 7986
3631.46	35257 - 7728
3647.84	34782 - 7377
3906.48	26479 - 888
3920.26	26479 - 978

C. Selection of Transition Probability Data

There are several well known compilations of iron transition probability data. Relevant information on these compilations is summarized in Table 9. All of these authors reported absolute values.

Table 9. Compilations of Fe transition probabilities

Investigators	How obtained	Identification
Corliss and Tech (54)	Average of most reliable values	CT
King and King (55)	Absorption in furnace	KK
Crosswhite (56)	Flame emission measurements[a]	C
Corliss and Bozman (57)	Arc emission measurements	CB
Valters and Startsev (58)	Hook method	VS

[a]A few of Crosswhite's values were taken from KK.

D. Experimental Facilities and Procedures

The experimental facilities and operating conditions were the same as those employed in the preceding section. The set of Fe solutions employed was prepared by dissolving pure Fe in HCl followed by dilution to the desired concentration with water.

Curves of growth were determined for each line of interest and the best solution concentration for each one of them was selected. Then, the spectral line intensities were measured at these concentrations. The spectrometer calibration factors were also measured by means of calibrated tungsten strip lamps and Equation 31.

A computer program was written to perform the necessary calculations to provide a straight line in the temperature plot with a least squares fit to the experimental data. The slope temperatures were also calculated by this program.

E. Results and Discussion

The result of temperature measurements by the slope method using the two groups of Fe lines and several published sets of transition probabilities is shown in Figure 10. The result of a reversal temperature measurement with the 3719.94Å Fe ground state line is also shown. The reversal temperature corresponds to the temperature experienced by the Fe atoms in this particular flame-burner system, as explained previously.

A range of more than 120°K is shown when either group of Fe lines is employed with the 5 different sets of transition probabilities. A lack of self-consistency is also shown because a different temperature value is obtained for each group of lines even if the same set of transition probabilities is

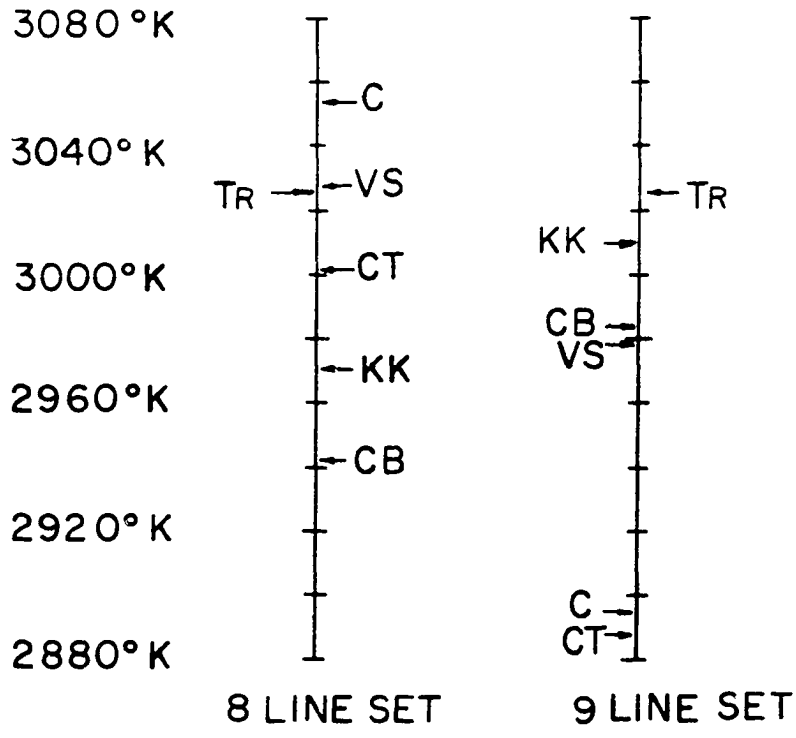

Fig. 10. Result of temperature measurements in a N_2O-C_2H_2 flame by the slope method using two groups of Fe lines and several published sets (see Table 9) of transition probabilities. The result of a reversal temperature measurement (T_R) is also shown

employed. These uncertainties in the measurement of the flame temperature are intolerable if accurate studies of flame processes and equilibria or measurements of important physical parameters are intended.

The results of this study stress then the need for an accurate set of Fe relative transition probabilities to be used for temperature measurements by the slope method. The experimental determination of these useful parameters is considered in the next section.

VII. EXPERIMENTAL DETERMINATION OF ACCURATE RELATIVE TRANSITION PROBABILITIES FOR Fe

Precise relative transition probabilities can in principle be measured if (a) the thermometric species reside only in an isothermal temperature field, (b) the temperature of this field is accurately determined by a technique which does not require of transition probability data, such as the reversal method, and (c) integrated line radiances or quantities strictly proportional to them are accurately measured under conditions of negligible self-absorption. Sections V and VI have shown that all of these requirements are met in our experimental system when Fe is employed as the thermometric species. Thus, Fe relative transition probabilities were experimentally determined as follows.

The integrated radiance emitted by a spectral line under conditions of negligible self-absorption has been shown to be

$$B(em) = \frac{1}{4\pi} A_{qp} \, h\nu_o \, n_q \, \ell \qquad (20)$$

Making use of the Boltzmann distribution equation, then

$$B(em) = \frac{1}{4\pi} A_{qp} \, h\nu_o \, \frac{g_q}{g_o} \, n_o \, e^{-E_q/kT_f} \, \ell \qquad (34)$$

If accurate values for B(em), T_f, ℓ and n_o could be measured, then the absolute value of the transition probability A_{qp} would be obtained. However, the value of n_o in the

flame is not known and consequently, only relative values can be determined. If Equation 34 is applied to two spectral lines and the result rearranged, the following relationship is obtained,

$$\frac{A_{q'p'}}{A_{qp}} = \frac{n_o}{n_o'} \frac{g_q}{g_{q'}} \frac{\nu}{\nu'} \frac{B'(em)}{B(em)} e^{-(E_q - E_{q'})/kT_f} \qquad (35)$$

where n_o/n_o' is the ratio of the number density of free atoms in the ground state at the two solution concentrations, c_s and c_s', which have been found appropriate to yield integrated line radiances, B(em) and B'(em), without appreciable self-absorption. Thus, only values of T_f, n_o/n_o' and $B'(em)/B(em)$ are needed to obtain relative atomic transition probabilities.

The flame temperature can be obtained by means of the reversal technique. Since curves of growth with slope = 1 regions have been determined at all values of the solution concentrations employed, the degree of atomization is constant in this concentration range and the number density of free atoms in the flame is proportional to the solution concentration. Thus, the value of n_o/n_o' is given by the ratio of the solution concentrations c_s/c_s'. For isothermal non-homogeneous flames the value of $\overline{n_o}/\overline{n_o}'$ is required (see Equation 9), but this ratio is also equal to c_s/c_s'. The measurement of B'(em)/B(em) requires a spectral calibration of the spec-

trometer, as explained previously, and from Equations 32 and 33, this ratio of spectral line radiances is given by

$$\frac{B'(em)}{B(em)} = \frac{I^{meas}_{(cont)}}{I^{meas\,'}_{(cont)}} \frac{I^{meas\,'}_{(em)}}{I^{meas}_{(em)}} \frac{\Delta\nu'}{\Delta\nu} \frac{B^{b}_{\nu}(\nu_o', T_b')}{B^{b}_{\nu}(\nu_o, T_b)} \tag{36}$$

Introducing these considerations into Equation 35, the following result is obtained for the transition probability ratio

$$\frac{A_{q'p'}}{A_{qp}} = \frac{c_s}{c_s'} \frac{g_q}{g_{q'}} \frac{\nu}{\nu'} \frac{I^{meas}_{(cont)}}{I^{meas}_{(cont)'}} \frac{I^{meas}_{(em)}}{I^{meas}_{(em)'}} \frac{\Delta\nu'}{\Delta\nu} \frac{B^{b}_{\nu}(\nu_o', T_b')}{B^{b}_{\nu}(\nu_o, T_b)} e^{\frac{-(E_q - E_{q'})}{kT_f}} \tag{37}$$

If the expression for the blackbody spectral radiance, approximated by Wien's law,

$$B^{b}_{\nu}(\nu_o, T_b) = \frac{c}{4\pi} \frac{8\pi h \nu_o^{3}}{c^{3}} e^{-h\nu_o/kT_b}$$

is introduced in Equation 37, the final result is

$$\frac{A_{q'p'}}{A_{qp}} = \frac{c_s}{c_s'} \frac{g_q}{g_{q'}} \left(\frac{\nu'}{\nu}\right)^2 \frac{I^{meas}_{(cont)}}{I^{meas\,'}_{(cont)}} \frac{I^{meas\,'}_{(em)}}{I^{meas}_{(em)}} \frac{\Delta\nu'}{\Delta\nu} e^{\frac{-(E_q - E_{q'})}{kT_f}} e^{\frac{+(E_q - E_p)}{kT_b}} e^{\frac{-(E_{q'} - E_{p'})}{kT_{b'}}} \tag{38}$$

where $h\nu_o$ and $h\nu_o'$ have been substituted by $(E_q - E_p)$ and $(E_{q'} - E_{p'})$.

A total of 43 iron lines were selected for this study based on criteria mentioned in the previous section. The experimental facilities and operating conditions were also the same as described previously, with the exception that the burner port was not water cooled.

Three independent relative transition probability determinations were performed by using three different calibrated tungsten strip lamps and sets of Fe solutions. Each lamp was calibrated several times with the optical pyrometer and an average value was taken. The single determinations for all the lamps did not differ by more than 5°K from the average value.

The Fe 3734.87Å line was selected as a reference intensity to assure maximal accuracy in the transition probability measurements. Measurements on the relative intensity of this line and the others of interest were alternated. In this way, intensity ratios were actually measured and the effect of any fluctuations in the system was minimized. These intensity ratios were measured at least three times and an average value was taken. The reversal temperature determinations were performed on the 3719.94Å ground state line. The reversal temperatures did not show any variation, within the experimental error of 10°K, with time.

The iron temperature field in the flame measured by each one of the lamps was 3084, 3074 and 3077°K. The average

values obtained for the relative transition probabilities by means of Equation 38 are shown in Table 10. The single measurements did not deviate by more than 3% from the average value, and actually most of them differed by 1% or less. As a comparison, relative transition probabilities from a recent publication by Corliss and Tech (54), whose values are the average of the best ones available, are also shown in Table 10.

The importance of the data presented in Table 10 can be illustrated by calculating the temperatures that would be obtained for a given spectral source when some of the Fe line pairs recommended in the literature for two-line temperature measurements are used. Table 11 shows the result of temperature calculations employing CT transition probabilities when the transition probabilities obtained in this work yield a temperature of 3000°K. Many similar examples can be given.

Thus, the determination of accurate relative transition probabilities for 43 Fe lines in the 3450-3950Å wavelength region will increase significantly the accuracy of temperature measurements in isothermal flames.

Table 10. Relative transition probabilities for 43 Fe lines with respect to the 3734.87Å line

Wavelength (Å)	Energy levels (cm^{-1})	Relative transition probabilities This work	[CT]
3465.86	29733- 888	0.124	0.131
3475.45	29469- 704	0.0990	0.0987
3476.40	29733- 978	0.0591	0.0655
3490.58	29056- 416	0.0637	0.0483
3497.84	29469- 888	0.0295	0.0361
3565.38	35768-7728	0.435	0.463
3570.10	35379-7377	0.775	0.722
3581.20	34844-6928	1.16	0.981
3608.86	35856-8155	0.905	1.12
3618.77	35612-7986	0.751	0.858
3631.46	35257-7728	0.560	0.576
3647.84	34782-7377	0.331	0.388
3679.92	27167- 0	0.0153	0.0169
3687.46	34040-6928	0.0879	0.114
3705.57	27395- 416	0.0365	0.0341
3709.25	34329-7377	0.170	0.214
3719.94	26875- 0	0.181	0.129
3722.56	27560- 704	0.0556	0.0567
3727.62	34547-7728	0.237	0.297
3733.32	27666- 888	0.0692	0.0646
3734.87	33695-6928	1.00	1.00
3737.13	27167- 416	0.157	0.104
3743.36	34692-7986	0.276	0.447
3748.26	27560- 888	0.0997	0.0790
3749.49	34040-7377	0.839	0.895
3758.24	34329-7728	0.691	0.852
3763.79	34547-7986	0.587	0.747
3767.19	34692-8155	0.681	0.923
3795.00	34329-7986	0.123	0.170
3815.84	38175-11976	1.09	1.61
3820.43	33096-6928	0.718	0.809
3824.44	26140- 0	0.0311	0.0272
3825.88	33507-7377	0.641	0.729
3834.22	33802-7728	0.471	0.573
3856.37	26340- 416	0.0503	0.0401
3859.91	25900- 0	0.106	0.0826
3895.66	26550- 888	0.0994	0.0988
3899.71	26340- 704	0.0280	0.0259

Table 10. (Continued)

Wavelength (Å)	Energy levels (cm^{-1})	Relative transition probabilities This work	[CT]
3906.48	26479- 888	0.00897	0.0108
3920.26	26479- 978	0.0276	0.0296
3922.91	25900- 416	0.0117	0.0108
3927.92	26340- 888	0.0263	0.0267
3930.30	26140- 704	0.0206	0.0187

Table 11. Two-line temperature calculations

Line pairs (Å)	Temperatures obtained with transition probabilities by CT	This work
3734.87-3737.13 (59)	2651	3000
3834.22-3895.66 (18)	2835	3000
3497.84-3570.10 (18)	3319	3000

VIII. BIBLIOGRAPHY

1. de Galan, L. and J. D. Winefordner, J. Quant. Spectrosc. Radiat. Transfer, 7, 703 (1967).

2. Kirkbright, G. F., M. K. Peters, M. Sargent and T. S. West, Talanta, 15, 663 (1968).

3. de Galan, L. and G. F. Samaey, Spectrochimica Acta, 25B, 245 (1970).

4. Snelleman, W. and J. A. Smit, Metrologia, 4, 123 (1968).

5. Snelleman, W., Combustion and Flame, 11, 453 (1967).

6. Snelleman, W., in Flame Emission and Atomic absorption Spectrometry, Volume 1 - Theory, Dean, J. A. and T. C. Rains, Eds., Marcel Dekker, Inc., New York, N.Y., 1969, Chapter 7.

7. Penner, S. S., Quantitative Molecular Spectroscopy and Gas Emissivities, Addison-Wesley Publishing Company, Inc., Reading, Massachusetts, 1959.

8. Thomas, D. L., Combustion and Flame, 12, 541 (1968).

9. Greig, J. R., Brit. J. Appl. Phys., 16, 957 (1965).

10. Silverman, S., J. Opt. Soc. Am., 39, 275 (1949).

11. Tourin, R. H., Spectroscopic Gas Temperature Measurement, Elsevier Publishing Company, New York, N.Y., 1966.

12. Bell, E. E., P. B. Burnside and F. P. Dickey, J. Opt. Soc. Am., 50, 1286 (1960).

13. Babrov, H. J., J. Opt. Soc. Am., 51, 171 (1961).

14. Hinnov, E. and H. Kohn, J. Opt. Soc. Am., 47, 156 (1957).

15. Gaydon, A. G., The Spectroscopy of Flames, Chapman and Hall Ltd., London, England, 1957.

16. Boumans, P. W. J. M., Theory of Spectrochemical Excitation, Hilger and Watts Ltd., London, England, 1966.

17. Broida, H. P. and K. E. Shuler, J. Chem. Phys., 27, 933 (1957).

18. Kirkbright, G. F., M. Sargent and S. Vetter, Spectrochimica Acta, 25B, 465 (1970).

19. Sasaki, Y., Jap. J. Appl. Phys., 5, 439 (1966).

20. Kadyshevich, A. E., Usp. Fiz. Nauk., 76, 683 (1962).

21. Hefferlin, R. and J. Gearhart, J. Quant. Spectrosc. Radiat. Transfer, 4, 9 (1964).

22. Hefferlin, R., J. Quant. Spectrosc. Radiat. Transfer, 5, 425 (1965).

23. Hefferlin, R., J. Quant. Spectrosc. Radiat. Transfer, 9, 1033 (1969).

24. Desai, S. V. and W. H. Corcoran, J. Quant. Spectrosc. Radiat. Transfer, 8, 1721 (1968).

25. Gusinow, M. A., J. B. Gerardo and R. A. Hill, J. Quant. Spectrosc. Radiat. Transfer, 9, 383 (1969).

26. Warner, B. and C. R. Cowley, J. Quant. Spec. Radiat. Transfer, 7, 751 (1967).

27. Tourin, R. H. and B. Krakow, Applied Optics, 4, 237 (1965).

28. Krakow, B., Applied Optics, 5, 201 (1966).

29. Strong, H. M. and F. P. Bundy, J. Appl. Phys., 25, 1521 (1954).

30. Drawin, H. W. and P. Felenbok. Data for Plasmas in Local Thermodynamic Equilibrium, Gauthier-Villars, Paris, France, 1965.

31. Hollander, T., Amer. Inst. Aeronaut. Astronaut. J., 6, 385 (1968).

32. Alkemade, C. Th. J., in Tenth Colloquium Spectroscopicum Internationale, Lippincott, E. R. and M. Margoshes, Eds., Spartan Books, Washington, D.C., 1963.

33. Gaydon, A. G. and H. G. Wolfhard, Flames, Their Structure, Radiation and Temperature, 2nd edition, Chapman and Hall Ltd., London, England, 1960.

34. Griem, H. R., Plasma Spectroscopy, McGraw-Hill Book Company, New York, N.Y., 1964.

35. Mitchell, A. C. G. and M. W. Zemansky, Resonance Radiation and Excited Atoms, Cambridge University Press, New York, N.Y., 1934.

36. Hinnov, E., J. Opt. Soc. Am., 47, 151 (1957).

37. Hofmann, F. W. and H. Kohn, J. Opt. Soc. Am., 51, 512 (1961).

38. Kalff, P. J., Tj. Hollander and C. Th. J. Alkemade, J. Chem. Phys., 43, 2299 (1965).

39. Snelleman, W. A flame as a standard of temperature. Unpublished Ph.D. thesis. Utrecht, Holland, University of Utrecht. 1965.

40. Alkemade, C. Th. J. A contribution to the development and understanding of flame photometry. Unpublished Ph.D. thesis. Utrecht, Holland, University of Utrecht. 1954.

41. Cowley, T. G., V. A. Fassel and R. N. Kniseley, Spectrochimica Acta, 23B, 771 (1968).

42. Fassel, V. A., J. O. Rasmuson, R. N. Kniseley and T. G. Cowley, Spectrochimica Acta, 25B, 559 (1970).

43. Maldonado, C. D., A. P. Caron and H. N. Olsen, J. Opt. Soc. Am., 55, 1247 (1965).

44. Maldonado, C. D. and H. N. Olsen, J. Opt. Soc. Am., 56, 1305 (1966).

45. Maldonado, C. D., J. Opt. Soc. Am., 57, 1231 (1967).

46. Olsen, H. N., C. D. Maldonado and G. D. Duckworth, J. Quant. Spectrosc. Radiat. Transfer, 8, 1419 (1968).

47. Fiorino, J. A., R. N. Kniseley and V. A. Fassel, Spectrochimica Acta, 23B, 413 (1968).

48. de Vos, J. C., Physica, 20, 690 (1954).

49. Glennon, B. M. and W. L. Wiese, Bibliography on Atomic Transition Probabilities, National Bureau of Standards, Monograph 50 (1962).

50. Glennon, B. M. and W. L. Wiese, Bibliography on Atomic Transition Probabilities, National Bureau of Standards, Miscellaneous Publication 278 (1966).

51. Glennon, B. M. and W. L. Wiese, Bibliography on Atomic Transition Probabilities, National Bureau of Standards, Miscellaneous Publication 278-Supplement (1968).

52. Seshadri, K. S. and R. N. Jones, Spectrochimica Acta, 19, 1013 (1963).

53. Reif, I., R. N. Kniseley and V. A. Fassel, Applied Optics, 9, 2398 (1970).

54. Corliss, C. M. and J. L. Tech, Oscillator Strengths and Transition Probabilities for 3288 Lines of FeI, National Bureau of Standards, Monograph 108 (1968).

55. King, R. B. and A. S. King, Astrophys. J., 87, 24 (1938).

56. Crosswhite, H. M. The spectrum of FeI. Johns Hopkins Spectroscopic Report Number 13. The Johns Hopkins University, Baltimore, Maryland. 1958.

57. Corliss, C. H. and W. R. Bozman, Experimental Transition Probabilities for Spectral Lines of Seventy Elements, National Bureau of Standards, Monograph 53 (1962).

58. Valters, A. K. and G. P. Startsev, Opt. Spectry., 17, 262 (1964). (English translation).

59. Winefordner, J. D., C. T. Mansfield and T. J. Vickers, Analytical Chemistry, 35, 1611 (1963).

IX. ACKNOWLEDGMENTS

I gratefully acknowledge the guidance and assistance provided by Dr. Velmer A. Fassel during the course of this thesis research. I also would like to express my personal thanks to Richard N. Kniseley for the many stimulating and helpful discussions which facilitated the completion of this investigation.

Above all, I wish to express my gratitude for the love, encouragement and understanding of my wife Sara and my daughter Tania to whom I dedicate this work.

X. APPENDIX A

The expression for the "slope temperature" is derived as follows:

$$\frac{1}{kT_{slope}(E_q)} = \frac{\partial}{\partial E_q} \frac{E_q}{k\dot{T}(E_q)}$$

$$\frac{\partial}{\partial E_q}\left(\frac{E_q}{k\dot{T}(E_q)}\right) = -\frac{k\dot{T}(E_q) - \left(\frac{\partial k\dot{T}(E_q)}{\partial E_q}\right) E_q}{\left(k\dot{T}_{(E_q)}\right)^2} \qquad \text{(A-1)}$$

but

$$e^{-E_q/k\dot{T}(E_q)} = \frac{\int_o^\ell dx\, n_o(x)\, e^{-E_q/kT(x)}}{\int_o^\ell dx\, n_o(x)}$$

and

$$k\dot{T}_{(E_q)} = -\frac{E_q}{\ln\left(\frac{\int_o^\ell dx\, n_o(x)\, e^{-E_q/kT(x)}}{\int_o^\ell dx\, n_o(x)}\right)}$$

so

$$\frac{\partial(k\dot{T}_{(E_q)})}{\partial E_q} =$$

$$\ln\left(\frac{\int_o^{\ell} dx\, n_o(x)\, e^{-E_q/kT(x)}}{\int_o^{\ell} dx\, n_o(x)}\right) + E_q\left(\frac{\int_o^{\ell} dx\, n_o(x)\, \frac{1}{kT(x)} e^{-E_q/kT(x)}}{\int_o^{\ell} dx\, n_o(x)\, e^{-E_q/KT(x)}}\right)$$

$$- \frac{}{\left[\ln\left(\frac{\int_o^{\ell} dx\, n_o(x)\, e^{-E_q/kT(x)}}{\int_o^{\ell} dx\, n_o(x)}\right)\right]^2}$$

If this expression is substituted in Equation (A-1) and the result simplified, then

$$\frac{1}{T_{slope}} = \frac{\int_o^{\ell} dx\, n_o(x) \frac{1}{T(x)}\, e^{-E_q/kT(x)}}{\int_o^{\ell} dx\, n_o(x)\, e^{-E_q/kT_{(x)}}}$$

XI. APPENDIX B

In this appendix the result of an emission measurement using an exit slit larger than the entrance slit is derived. The derivation follows closely Penner's for related cases (7).

The slit function of the spectrometer entrance slit where the instrument shows some response to the frequency ν' when the exit slit is set at ν will be called $g(|\nu'-\nu|)$. The slit function vanishes for $\nu'-\nu \geq \Delta\nu^*$. We will consider the spectral region between ν_1 and ν_2 ($\nu_1 < \nu_2$) which contains a single spectral line. The frequencies ν_1 and ν_2 are selected in such a way that the spectral absorptivity $\alpha_\nu(\nu)$ of the line, which is defined as $\alpha_\nu(\nu) = (1-e^{-K(\nu)\ell})$ (see Equation 6), vanishes at $\nu < \nu_1 + \Delta\nu^*$ and for $\nu > \nu_2 - \Delta\nu^*$. Then, the image of the entrance slit will be described by

$$\int_{\nu-\Delta\nu^*}^{\nu+\Delta\nu^*} [B^b_{\nu'}(\nu', T_f)\, \alpha_{\nu'}(\nu')]\, g(|\nu'-\nu|)\, d\nu'$$

This function will vanish at $\nu \geq \nu_2$ and $\nu \leq \nu_1$. If the exit slit is longer than the image of the entrance slit, then the signal detected will be given by

$$I^{meas}_{(em)} = \int_{\nu_1^*}^{\nu_2^*} \int_{\nu-\Delta\nu^*}^{\nu+\Delta\nu^*} [B^b_{\nu'}(\nu', T_f)\alpha_{\nu'}(\nu')]g(|\nu'-\nu|)d\nu'\, d\nu$$

where $\nu_2^* > \nu_2$ and $\nu_1^* < \nu_1$. The blackbody spectral radiance

is essentially constant in the frequency range considered, so $B^b_{\nu'}(\nu', T_f) = B^b_{\nu}(\nu_o, T_f)$ where ν_o is the frequency at the center of the line. If the change of variables $\tau = \nu' - \nu$ is introduced and the order of integration is changed, then

$$I^{meas}_{(em)} = B^b_{\nu}(\nu_o, T_f) \int_{\nu_1^*}^{\nu_2^*} \int_{-\Delta\nu^*}^{+\Delta\nu^*} \alpha_{\nu'}(\nu+\tau)\, g(|\tau|)\, d\tau\, d\nu$$

or

$$I^{meas}_{(em)} = B^b_{\nu}(\nu_o, T_f) \int_{-\Delta\nu^*}^{+\Delta\nu^*} g(|\tau|) \left[\int_{\nu_1^*+\tau}^{\nu_2^*+\tau} \alpha_{\nu}(\nu)\, d\nu \right] d\tau$$

However, since $|\tau| \leq \Delta\nu^*$, the stated requirements for $\alpha_\nu(\nu)$ imply that

$$\int_{\nu_1^*+\tau}^{\nu_2^*+\tau} \alpha_\nu(\nu)\, d\nu = \int_{\nu_1}^{\nu_2} \alpha_\nu(\nu) d\nu = \alpha$$

Then,

$$I^{meas}_{(em)} = B^b_{\nu}(\nu_o, T_f)\, \alpha \int_{-\Delta\nu^*}^{\Delta\nu^*} g(|\tau|) d\tau = B^b_{\nu}(\nu_o, T_f) \alpha\, G \qquad \text{(B-1)}$$

where G stands for the integral of the slit function.

To determine the value of G, light from a calibrated tungsten lamp is focused on the entrance slit of the spectrometer. The signal detected is now given by

$$I^{meas}_{(cont)} = \int_{\nu_1^*}^{\nu_2^*} \int_{\nu-\Delta\nu^*}^{\nu+\Delta\nu^*} [B^b_{\nu'}(\nu', T_b)]\, g(|\nu'-\nu|)\, d\nu'\, d\nu$$

Following the same arguments as before,

$$I^{meas}_{(cont)} = B^b_\nu(\nu_o, T_b)\ (\nu_2^* - \nu_1^*)G \qquad \text{(B-2)}$$

Therefore,

$$\frac{I^{meas}_{(em)}}{I^{meas}_{(cont)}} = \frac{\alpha\ B^b_\nu(\nu_o, T_f)}{(\nu_2^* - \nu_1^*)\ B^b_\nu(\nu_o, T_b)}$$

or

$$I^{meas}_{(em)} = C_{(\nu)}\ \alpha\ B^b_\nu(\nu_o, T_f) = C_{(\nu)}\ B_{(em)}$$

where

$$C_{(\nu)} = \frac{I^{meas}_{(cont)}}{(\nu_2^* - \nu_1^*)\ B^b_\nu(\nu_o, T_b)}$$

To determine the value of $(\nu_2^* - \nu_1^*)$, i.e. the bandpass of the instrument, a spectral line is scanned and the area under the curve is divided by the peak intensity. The peak intensity is given by Equation B-1 and the area under the curve is given by (7),

$$\text{Area} = B^b_\nu(\nu_o, T_f)\ \alpha\ G'$$

where G' stands for the integral of the slit function of the entrance and exit slits. Then,

$$\frac{\text{Area}}{\text{Peak}} = \frac{B_\nu{}^b(\nu_o, T_f) \;\alpha\; G'}{B_\nu{}^b(\nu_o, T_f) \;\alpha\; G} = \frac{G'}{G}$$

Now, if a continuum source were focused on the slit, the signal produced can be written as (see Equation B-2),

$$I^{meas}_{(cont)} = B^b_\nu(\nu_o, T_b)\ (\nu_2{}^* - \nu_1{}^*)\ G$$

or (7)

$$I^{meas}_{(cont)} = B_\nu{}^b(\nu_o, T_b)\ G'$$

therefore,

$$\frac{G'}{G} = (\nu_2{}^* - \nu_1{}^*)$$

and

$$\frac{\text{Area}}{\text{Peak}} = (\nu_2{}^* - \nu_1{}^*)$$